Available online at www.sciencedirect.com

ScienceDirect

Journal of Magnesium and Alloys xxx (xxxx) xxx

www.elsevier.com/locate/jma

Review

Antibacterial mechanism with consequent cytotoxicity of different reinforcements in biodegradable magnesium and zinc alloys: A review

Chowdhury Ahmed Shahed[a], Faiz Ahmad[a,*], Ebru Günister[b], Farhana Mohd Foudzi[c], Saad Ali[a], Khurshid Malik[a], Wan Sharuzi Wan Harun[d]

[a] *Department of Mechanical Engineering, Universiti Teknologi PETRONAS (UTP), 32610, Seri Iskandar, Perak, Malaysia*
[b] *Faculty of Engineering and Natural Sciences, Department of Mechanical Engineering, Istanbul Health and Technology University, Istanbul, Turkey*
[c] *Department of Mechanical and Manufacturing Engineering, Faculty of Engineering and Built Environment, Universiti Kebangsaan Malaysia, 43600 UKM Bangi, Selangor, Malaysia*
[d] *Faculty of Mechanical & Automotive Engineering Technology, Universiti Malaysia Pahang, 26600 Pekan, Pahang, Malaysia*

Received 19 June 2023; received in revised form 6 August 2023; accepted 23 August 2023
Available online xxx

Abstract

Benefits achieved by the biodegradable magnesium (Mg) and zinc (Zn) implants could be suppressed due to the invasion of infectious microbial, common bacteria, and fungi. Postoperative medications and the antibacterial properties of pure Mg and Zn are insufficient against biofilm and antibiotic-resistant bacteria, bringing osteomyelitis, necrosis, and even death. This study evaluates the antibacterial performance of biodegradable Mg and Zn alloys of different reinforcements, including silver (Ag), copper (Cu), lithium (Li), and gallium (Ga). Copper ions (Cu^{2+}) can eradicate biofilms and antibiotic-resistant bacteria by extracting electrons from the cellular structure. Silver ion (Ag^{+}) kills bacteria by creating bonds with the thiol group. Gallium ion (Ga^{3+}) inhibits ferric ion (Fe^{3+}) absorption, leading to nutrient deficiency and bacterial death. Nanoparticles and reactive oxygen species (ROS) can penetrate bacteria cell walls directly, develop bonds with receptors, and damage nucleotides. Antibacterial action depends on the alkali nature of metal ions and their degradation rate, which often causes cytotoxicity in living cells. Therefore, this review emphasizes the insight into degradation rate, antibacterial mechanism, and their consequent cytotoxicity and observes the correlation between antibacterial performance and oxidation number of metal ions.

Keywords: Biodegradable materials; Biomedical implants; Antibacterial mechanism; Cytotoxicity; Reactive oxygen species.

1. Introduction

A permanent implant is unfavorable for the pediatric patient as the metal implant cannot adjust to the recipient's body growth [1]. Temporary implants can be placed inside the body for a relatively shorter period to support the body structures and must be removed after finishing the task. The removal of these implants is unavoidable in such cases, and it can lead to challenges during the surgical procedure and potential postoperative complications. A biodegradable implant is a savior for this problem, where the body absorbs the implanted part gradually. Biodegradable implant materials (BIMs) can be fabricated using polymers, ceramics, composites, and metal. Among them, metals have superiority over others for their excellent mechanical properties. Metal is suitable for load-bearing applications where polymers are shy of fulfilling such requirements, and ceramics are brittle in nature with a very slow degradation rate. Again, the stress shielding effect hinders its progress due to the high elastic modulus. Composites have the potential in the bio-implant sector since the properties are highly dependent on the type of matrix and reinforcement(s) [2,3]. Although all metals are not well practiced as BIMs, Mg and Mg alloys, Zn and Zn alloys are the most suitable. These pure metals or alloys can be dissolved or absorbed in the body, thus exempting secondary implant

* Corresponding author.
E-mail address: faizahmad@utp.edu.my (F. Ahmad).

https://doi.org/10.1016/j.jma.2023.08.018

removal surgery. Researchers also developed ferrous (Fe) and Fe-based biodegradable alloys [4,5]; however, they possess a very slow degradation rate with a high modulus of elasticity that is not suitable when faster degradation is targeted [6]. Furthermore, according to Wolff's law, osteopenia and re-fracture are most likely to occur because of the mismatch of elastic modulus between human bone and artificial metal implant [7,8].

Iron-based implants are usually used in load-bearing applications with minute degradation and little toxicity. Mg and Zn are the principal alloying elements for developing such alloys [9]. Heavy metals are often considered not suitable for biomedical implants as they could react with the body fluid, enzymes, and proteins, resulting in toxicity [10]. For those reasons, Mg and Zn alloys are unequivocally popular in the field of degradable implants over other traditional biomedical implants. The nature of biodegradability of Mg alloys comes from the heart of being prone to corrosion in an aqueous solution, especially in body fluid [11,12]. Also, these materials must be macro or trace elements in the human body [13]. The degradation rate of Mg alloys is enormous and depends on the allowing elements, fabrication process, post-processing (heat treatment, coatings, and surface modification), and implant environment. A precipitated secondary phase may initiate micro-galvanic corrosion; thus, the dissolution of such a phase reduces the degradation rate [14]. Zhang et al. [15] conducted nanomodification on the surface of the Mg-0.2Cu alloy using surface mechanical grinding treatment, which induced nano-crystallization, and the modified surface exhibited a degradation rate that was one-ninth of the untreated surface during the first 12 h. Extruded Ni-reinforced Mg-Zn alloy degrades at a rate of 619 mm/y, whereas second-phase reinforcement of cerium and calcium shows relatively less degradation of around 1.5 mm/y for Mg-Zn alloys [16]. The major problems are the viscoelastic behavior, uncontrolled dissolution, and fast metal strength deterioration before the sufficient healing of the host tissue [17].

Most bioresorbable materials are broken into micro-pieces in an in-vivo environment and converted to essential metal ions, which can be carried out by blood circulation and absorbed by body cells [18]. Mg-based alloys like ZE21B [19], Zn-based allows like Zn-Ag [20], and Ca-Mg-Zn [21] have also been recently introduced to produce bioresorbable scaffolds, which are used as vascular implants, especially in arteries and veins [22–24]. Although pure Zn shows a lesser degradation rate of 0.063 mm y^{-1} after immersion for 336 h than Mg [25]; however, it causes a high level of inflammation [20]. Therefore, sodium hydroxide solution treatment, hydrofluoric acid (HFA) treatment, and sulfonated hyaluronic acid nanoparticles (S-HLA NPs) with poly L-lactic acid hybrid coating help to improve hemocompatibility and reduced corrosion rate [19,26]. The formation of MgF_2 passivation layer due to HFA treatment compounded with dopamine polymer film and hyaluronic acid loaded astaxanthin (HLA-ASTA) coating showed improved biocompatibility with increased endothelial cell proliferation [27].

Bacterial infection and biofilm formation on the implant site are recurrent problems and create significant complications. Biofilm construction prevents the antibiotics and immune response leading to inflammation, osteomyelitis, necrosis, and repetitive or implant correction surgery [28,29]. Osteomyelitis inhibits osseointegration (structural and functional integration between the metallic implant and living bone). It initiates osteoclast (cells that mediate bone loss by bone resorption), and the dominant bacteria for osteomyelitis are *Staphylococcus aureus* (*S. aureus*) and *Staphylococcus epidermidis* (*S. epidermidis*) [30]. Treatments include antibiotics, debridement, and filling the space after debridement help to eradicate bacteria [31]. The situation becomes worse when antibiotic-resistant bacteria, e.g., methicillin-resistant *Staphylococcus aureus* (MRSA) and methicillin-resistant *Staphylococcus epidermidis* (MRSE), attack the implanted site or biofilm have formed [32]. Thus, a robust antibacterial property is urgent for bioimplants.

In contrast, a robust antibacterial material often influences cytotoxicity in a living cell, which is incompatible with biomedical applications [33]. Mg and Zn-alloys implants are mainly coronary stents, bone fixation plates and screws, dental wire and membranes, craniomaxillofacial implants, surgical staples, and sutures [34,35], where outstanding cytocompatibility is obligatory. Unlike bone implants, cardiovascular stents are typically designed for temporary placement to maintain vessel patency. Also, these implants are in contact with continuous blood flow to maintain a sterile environment, making it challenging to form bacterial colonies, and the blood-carried immune cells defend against infection [36]. However, Infections on the implant sites can occur due to prolonged indwelling, restenosis (re-narrowing of the vessel), immunocompromising, and bacteremia (the presence of bacteria in the bloodstream) [37]. Thus, materials with antibacterial properties are handy for cardiovascular materials but not as crucial as orthopedic implants. Most bacteria-killing action is equally responsible for killing healthy body cells. Several studies have been published on the influence of fabrication techniques, mechanical performance, degradation mechanisms, and complications after implantation [38–47]. Yet, a detailed review regarding antibacterial mechanisms and the consequent cytotoxicity for commonly used alloying components, particularly in Mg and Zn alloys, is currently inadequate, leaving sufficient room for further discussion. Hence, this study aims to critically analyze the antibacterial mechanism and relevant cytotoxicity, giving the researchers a detailed understanding of potential harm to bodily cells. It will help predict and develop an effective implant material with effective antibacterial properties and minimal cytotoxic reaction. Furthermore, it discusses a correlation between metal ion's intrinsic chemical properties and antibacterial ability in Section 6, which will be helpful for researchers to perceive systematically.

2. Eligibility of Mg and Zn as biodegradable implants

Mg and its alloys provide a greater strength-to-weight ratio than metallic or polymeric bioimplants. The density of such

Please cite this article as: C.A. Shahed, F. Ahmad, E. Günister et al., Antibacterial mechanism with consequent cytotoxicity of different reinforcements in biodegradable magnesium and zinc alloys: A review, Journal of Magnesium and Alloys, https://doi.org/10.1016/j.jma.2023.08.018

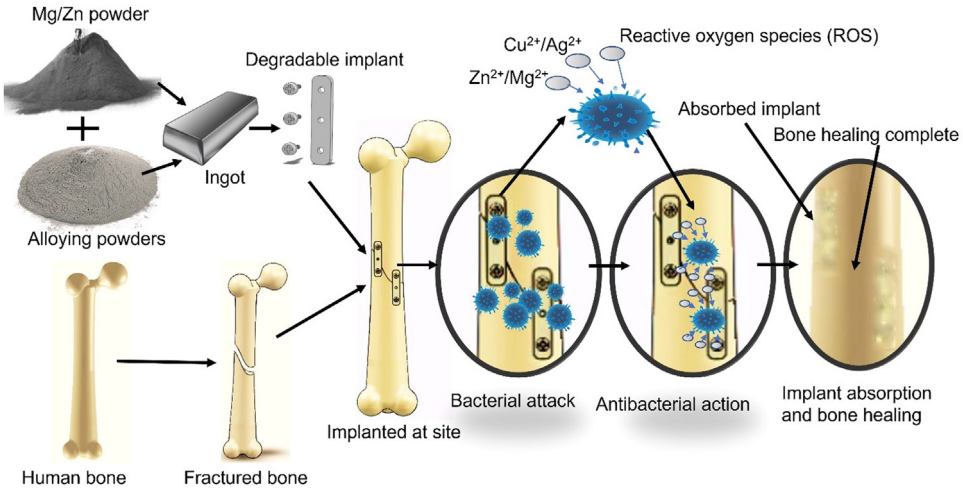

Fig. 1. Implants fabricated from Mg/Zn powders and alloying elements. Implants are implanted inside the body to support the site. Released metal ions take antibacterial action near the implant site, followed by site healing and completion of implant absorption.

alloys lies between 1.74–2.00 g/cm^3 and the elastic modulus 40–45 GPa, which is close to the human bone (1.8–2.1 g/cm^3 and 15–40 GPa). They also exhibit good vibration-damping properties, fatigue and creep strength, excellent thermal conductivity, high impact resistance, and good dimensional stability [48]. On the other hand, low fracture toughness, low compression strength (65–100 MPa) compared to femoral bone (∼162 MPa), poor ductility, and swift corroding nature in the physiological atmosphere (salty fluids, sugar, and proteins) restrict their applications [49,50]. The biggest challenge for Mg implants is to control the degradation rate to maintain sufficient mechanical strength as long as the site is completely healed.

Zn is the second most abundant metal, one of the essential elements in the human body, and it serves as a co-factor in all six classes of enzymes and several classes of proteins. According to the School of Public Health, Harvard, the maximum limit for taking Zn is 40 mg for people over 19 years of age, although the recommended limit is 11 mg for men and 8 mg for women of the same age group [51]. Poor mechanical strength of pure Mg and Zn can be improved significantly by adding alloying elements, including, but not limited to, titanium (Ti), silver (Ag), copper (Cu), manganese (Mn), strontium (Sr), Fe. Furthermore, these alloys have considerably lower degradation rates than pure Mg and Zn, which makes them more biocompatible and implantable. Zn is cathodic in nature; therefore, it reacts with the environment and creates a strong protective compound for slowing down the degradation rate. During the degradation process, constituent metals release ions, and implants are absorbed gradually into the body along with site healing. Fig. 1 illustrates the complete procedure from fabrication to bioabsorption and bone healing with antibacterial actions for Mg and Zn alloys.

Cell adhesion with metallic implants and bioactivity depends on the hydrophilicity of the implant's surface. Researchers use hydrophilic elements and coatings and often modify the outer surface of constituents by chemical or thermal treatment to improve hydrophilicity that decreases water contact angle (WCA). Wang et al. [52] noticed 264.81% more cell proliferation after adding hydrophilic graphene with HA when culturing rat's MC3T3-E1 cells. They also observed a reduced contact angle of 15.38° from 29.85° with high surface energy. Besides, an Nd-YAG laser improves hydrophilicity and less bacterial (*S. aureus*) adhesion tendency on the metal surface [53]. The untreated pure Mg and pure Zn showed 46.55° [54] and 60° [55] WCA, respectively, indicating a high wettability and degradation tendency. Excessive degradation of Zn, Mg, and its alloys can be controlled by maintaining hydrophilicity. Liu et al. [56] treated the TZ51 Mg alloy with anodic oxidation and formed a hydrophobic surface with WCA 163°. This surface can also be converted to hydrophilic with a WCA 1°−5° by annealing, as higher temperatures can destabilize and remove oxide layers, enhancing wettability [57]. Peng et al. used diamond-like carbon coated on the Zn to increase the WCA to 90°. Wettability is vital for biocompatibility and for antimicrobial properties since it controls the degradation rate and the amount of constituent ions released inside the body. These ions are eventually responsible for antibacterial actions and cytotoxicity.

In addition to the preceding discussion, the suitability of magnesium (Mg) and zinc (Zn) and their alloys largely relies on their acceptance by the host body. Hypersensitivity reactions and immune rejection are two major reasons for implant failure, which is common for degradable implants due to their ions and debris released in the body [58]. Excessive debris causes coagulative and caseous necrosis and acts as an immune trigger [59]. On that note, many studies have evaluated the inflammatory and immune response for Mg and Zn alloys. Mg possesses antioxidant ability, and Mg^{2+} ions can inhibit inflammation by effectively decreasing ROS [60]. Even alloying by silver or gadolinium does not have an adverse impact on cell viability. Mg and its alloys produce ample M2 macrophage phenotype to alleviate inflammation [61]. Similarly, Zn and Zn alloys do not show an inflammatory response,

Please cite this article as: C.A. Shahed, F. Ahmad, E. Günister et al., Antibacterial mechanism with consequent cytotoxicity of different reinforcements in biodegradable magnesium and zinc alloys: A review, Journal of Magnesium and Alloys, https://doi.org/10.1016/j.jma.2023.08.018

although a tiny amount of Mg with Zn alloys shows a minor inflammatory response due to the formation of Mg_2Zn_{11} intermetallic and a higher degradation rate [62,63]. A similar response was observed for binary Zn-4Li and Zn-(1,3,5)Al alloys due to the intermetallic precipitation [64,65]. However, Mn-doped Calcium phosphate-coated Zn- 0.1Li [66] and Zn-0.8Cu [67] promoted positive M2 macrophages without any inflammatory responses. Thus, the immune response for Mg and Zn alloys is satisfactory as a degradable biomedical implant.

3. Degradation mechanism of Mg and Zn implant

The degradation rate is directly related to the implant strength. Mg has higher tensile strength than Zn, but the rapid degradation and hydrogen gas emission limit its application. Proper biocompatible reinforcement with oxidative nature can form the protective oxide layers and decrease the degradation rate. The targeted degradation rate of <20 μm/year is considered suitable for cardiovascular scaffolding [68]. Mg has a high physiological interaction and absorbability in the human body. The body saline is an aqueous solution that further promotes the dissolution of Mg [69]. High chloride ion concentration ignites the corrosion and emits H_2 gas that hampers the site healing and initiates necrosis [70]. Chloride ions react with $Mg(OH)_2$ and convert into more soluble $MgCl_2$. Some parts of $Mg(OH)_2$ can convert MgO and H_2O, and MgO works as an antibacterial element during the tissue regeneration process. The degradation reactions of Mg implants are given in Eqs. (1–4) [71].

$$Mg\ (s) + 2H_2O\ (aq) \rightarrow Mg^{2+} + 2OH^- + H_2\ (g) \quad (1)$$

$$Mg\ (s) + 2Cl^- \rightarrow MgCl_2\ (aq) \quad (2)$$

$$Mg(OH)_2\ (aq) + 2Cl^- \rightarrow MgCl_2\ (aq) \quad (3)$$

$$Mg(OH)_2\ (aq) \leftrightarrow MgO\ (s) + H_2O\ (aq) \quad (4)$$

Researchers found that the safe value for internal degradation is 0.5 mm/yr, while the degradation rate for Mg alloys is much higher [72,73]. Nidadavolu et al. [74] determined that the average degradation rate of Mg alloys is around 5 mm/yr (0.51 μm/day). Additionally, weight loss increased over time due to the increased surface area. The formula for weight loss due to degradation can be defined as [75]:

Weight loss, $W = D \times A \times t$; where D= degradation rate, A= active surface area, t= immersion time.

Unlike Mg, the degradation of Zn does not emit H_2; hence, it produces oxides and relevant compounds based on the site's attending elements, such as calcium (Ca), carbonates (CO_3^{2-}), chlorine, and phosphates (PO_4^{3-}). The degradation rate increases in an alkaline in-vivo environment, underscoring the vital influences of other elements. Eqs. (5–11) [76] describes the Zn degradation steps by reacting with chloride and biphosphate ions (HPO_4^{2-}) and forming soluble or insoluble products. Since the degraded products are either absorbed by the tissue or excreted from the body by the kidneys, the selected reinforcement might be nontoxic and biocompatible.

$$2Zn\ (s) + 2H_2O\ (l) + O_2 \rightarrow 2Zn(OH)_2\ (aq) \quad (5)$$

$$2Zn\ (s) \rightarrow 2Zn^{2+} + 4e^-\ \text{(Anodic reaction)} \quad (6)$$

$$2H_2O\ (l) + O_2 + 4e^- \rightarrow 4OH^-\ \text{(Cathodic reaction)} \quad (7)$$

$$Zn(OH)_2\ (aq) \rightarrow ZnO\ (s) + H_2O\ (l) \quad (8)$$

$$6Zn(OH)_2\ (aq) + Zn^{2+} + 2Cl^- \rightarrow 6Zn(OH)_2.\ ZnCl_2\ (aq) \quad (9)$$

$$4ZnO\ (s) + 4H_2O\ (l) + Zn^{2+} + 2Cl^- \rightarrow 4Zn(OH)_2.\ ZnCl_2\ (aq) \quad (10)$$

$$Zn^{2+} + 2HPO_4^{2-} + 2OH^- + 2H_2O \rightarrow Zn_3(PO_4)_2.\ 4H_2O\ \text{(crystalline solid)} \quad (11)$$

The degradation nature and rate vary based on the implant aspect ratio and in-vivo application. For the same implant materials, implanted inside the abdominal aorta and bone implant gives different degradation rates while calculating by using the weight loss to the duration of implantation [76]. Therefore, the cross-sectional area reduction to the implantation period mentioned in Eq. (12) [77] has been given uniformity.

$$\text{Cross} - \text{sectional degradation rate} = \frac{\sqrt{\frac{A_0}{\pi}} - \sqrt{\frac{A_t}{\pi}}}{t} \quad (12)$$

Where t is the total duration of implantation, A_0 and A_t are the cross-sectional area of the implant when time = 0 and time = t, respectively. Another approach is proposed by Li et al. [78], considering the volume difference over the surface area by using Eq. (13), where V_0 and V_t represent the initial and final volume, respectively. Mei et al. used almost the same following equation by taking the weight difference (W_0-W_t) instead of the volume difference [79].

$$\text{Corrosion rate} = \frac{(V_o - V_t)}{A \times t} \quad (13)$$

Another degradation rate can be calculated by measuring the concentration of released ions in the extraction medium over a specific period of incubation time, given in Eq. (14) [80]. This equation is mostly used for in-vitro measurement but can also be used for in-vivo degradation by quantifying the metal release in periprosthetic tissue, blood, urine, or serum [81].

$$\text{Degradation rate} = \frac{\left(C_{sample} - C_{fresh}\right) \times V)}{(A \times T)} \quad (14)$$

Please cite this article as: C.A. Shahed, F. Ahmad, E. Günister et al., Antibacterial mechanism with consequent cytotoxicity of different reinforcements in biodegradable magnesium and zinc alloys: A review, Journal of Magnesium and Alloys, https://doi.org/10.1016/j.jma.2023.08.018

where C_{sample} is the ion concentration (μg/mL) in the extraction medium, C_{fresh} is the ion concentration (μg/mL) in the original fresh medium. V is the solution volume (mL). A is the surface area (cm^2), and T is the incubation time (day).

Degradation rates in the in-vivo condition are much higher than in in-vitro conditions due to the complex biological environment, including different enzymes, proteins, and immune responses [82]. Mechanical stresses related to physical movement, physiological activities, and weight-bearing can further expedite the degradation [1]. Also, the rate cannot be the same throughout the implantation period. In the initial state, implants degrade faster, followed by slow degradation due to the formation of protective layers. A time-dependent volume-based calculation is recommended to conveniently and accurately estimate the degradation rate during in-vivo observation using CT (computed tomography) images.

4. Antibacterial properties of reinforcements and consequent cytotoxicity

Antibacterial property often comes with cytotoxic aftermath; henceforth, equilibrium is necessary for successful implementation. Inorganic metal elements, e.g., Ag, Cu, Zn, Ga [29]; inorganic coatings, e.g., oxide, nitride, diamond-like carbon [83]; organic coating, e.g., chitosan, tannic acid, polyurethane, and drug-eluting implant with antibiotics, peptides are used to enhance antibacterial properties [84,85]. The antibacterial mechanism is implied in incrementing Zn and Mg ions concentration through degradation, which develops a considerable osmotic pressure and kills bacteria by osmotic lysis [80,86]. Extraction medium also influences the degradation and ion release in in-vitro conditions. Fetal bovine serum (FBS) gives fewer cytotoxic effects for Mg implants due to the corrosion protection layer forms on the alloys with the reaction of HCO_3^-, HPO_4^{2-} ions [87]. In contrast, FBS causes more Zn^{2+} release than DMEM, McCoy's extraction medium, causing cytotoxicity [80].

When Mg degrades excessively, it leads to the production of an excessive amount of H_2 gas and hypermagnesemia. Additionally, the degradation of Mg results in the formation of Mg^{2+} and hydroxyl ions (OH-) in the body fluid, as indicated in Eq. (1). Although these ions contribute to the bactericidal effect, elevated concentrations of them can lead to cytotoxicity [88]. Similarly, when the Zn^{2+} concentration crosses the Zn tolerance limit of biological cells, it responds cytotoxic. High Zn ions create copper deficiency and toxicity, including brain tissue damage, a hindrance to neuronal development, and respiratory tract inflammation [89]. Besides, gastrointestinal tract infection causes epigastric pain, nausea, and diarrhea and elevates the risk of prostate cancer [90]. Furthermore, the particle size and type of compounds from the degradation implant create different cytotoxicity. ZnO particles with different

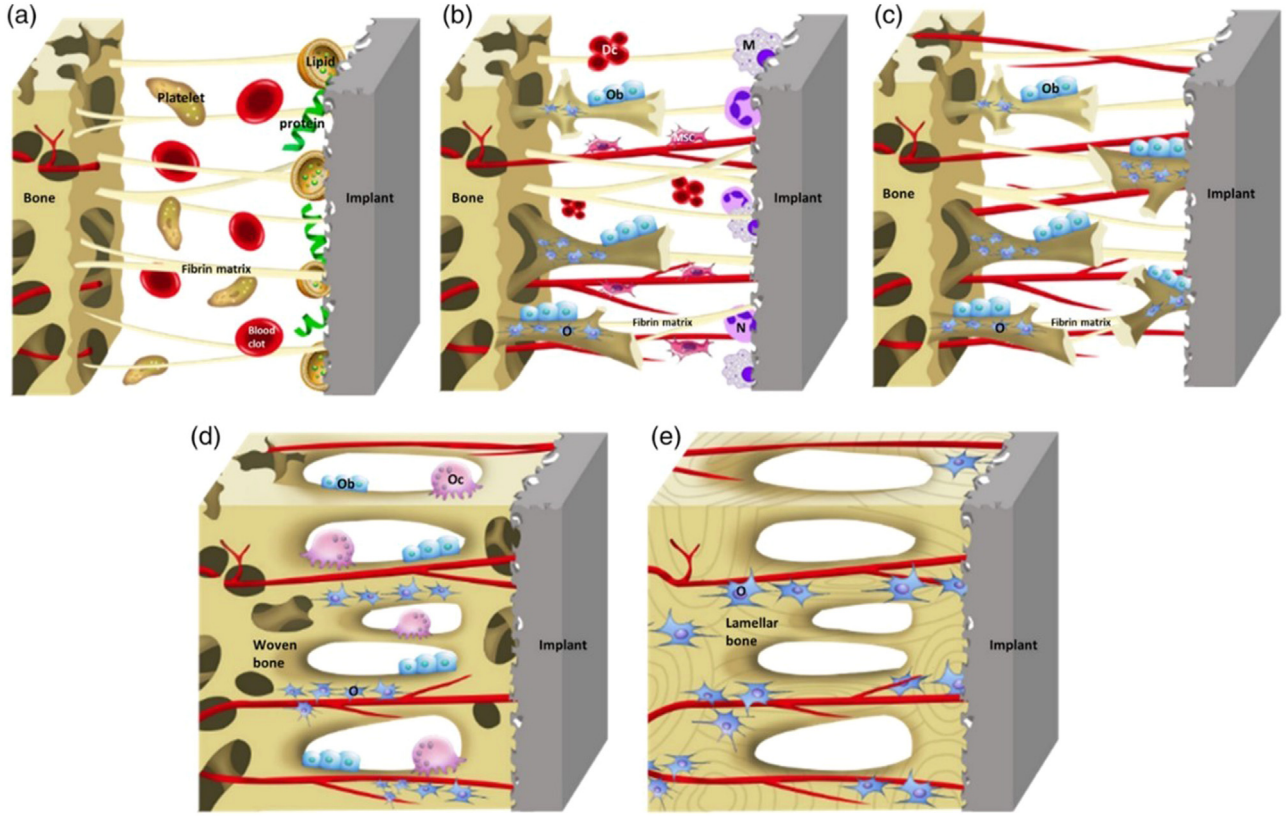

Fig. 2. Schematic of the osseointegration process starts with (a) the blood clot and fibrin matrix formation. (b) Angiogenesis and woven bone formation. (c) Distance and contact osteogenesis. (d) Fill up the gap with newly born woven bones and bone remodeling. (e) Woven bones transform into lamellar bones; (Reuse permission: open access) [102].

Please cite this article as: C.A. Shahed, F. Ahmad, E. Günister et al., Antibacterial mechanism with consequent cytotoxicity of different reinforcements in biodegradable magnesium and zinc alloys: A review, Journal of Magnesium and Alloys, https://doi.org/10.1016/j.jma.2023.08.018

sizes of 20 nm, 40 nm, and 80 nm have shown 67.7%, 83%, and 85% cell viability for L929 mouse fibroblast cells at a concentration of 200 μM [91], although the tolerance limit is less than 80 μM for Zn^{2+} ion concentration [92]. For human coronary artery endothelial and osteosarcoma U-2 cells, the tolerance limit is <100 μM [93] and < 120 μM [92], respectively.

Cytotoxicity hampers osteogenesis; therefore, controlled degradation is essential for bone formation. Mg degrades gradually inside the body and facilitates new bone generation. Xie et al. [94] developed Mg-Zn based alloy of ZK30-0.2Cu-xMn, where x = 0, 0.4, 0.8, 1.2, 1.6, and observed that all compounds demonstrated cytocompatibility under in-vitro conditions. Among these, ZK30-0.2Cu-0.8Mn exhibited better results in terms of degradation rate and antibacterial performance. Li et al. [95] tested the osteogenic performance of pure Mg, Mg-3 Zn, and Mg-2Zn-Mn. The Mg-2Zn-Mn showed stable degradation and excellent osteogenesis without systemic toxicity for rat's bone-tissue formation. Also, morphogenetic proteins of bones are observed with the involvement of fibroblast growth factor receptors. Surface modification plays a crucial role in enhancing biocompatibility. A porous structure with a proper three-dimensional surface network helps to improve osseointegration, cytocompatibility, and bone-implant integration. The porous implant framework facilitates nutrient and waste exchange, cellular infiltration, bone tissue integration, and vascularization. Scaffolds having pores ranging from 200 to 300 μm demonstrated superior osteogenesis due to the favorable spreading and elongation of stem cells [96]. Moreover, the presence of a nano-porous structure could potentially create a distinct immune environment, leading to alterations in macrophage morphology and the initiation of their osteoimmune response and improving bone regeneration [97].

On the other hand, material like lithium (Li) is well known for its osteogenesis and angiogenesis (promoting new blood vessel) capability [98]. Li-doped magnesium-phosphate bioceramic stimulates the osteogenic and angiogenic properties and has excellent potential in repairing bone defects [99]. Li activates the Canonical Wnt/β-catenin signaling (WCS) pathway, a pathway that regulates cell proliferation, migration, stem cell generation, and cell stability [100] and inhibits osteoclastogenesis [101]. Fig. 2 illustrates the osseointegration process of angiogenesis and bone remodeling, starting with developing a fibrin matrix involving various proteins and enzymes. After the formation of the fibrin matrix and new blood vessels, cell migration begins, and new woven bone forms. Gradually, the gap between the living bone and implant is closing, and the simultaneous action of osteoblast and osteoclast optimizes the lamellar bone surface [102].

To conclude, the synergistic effect of porous implants and suitable materials improves osseointegration efficacy. However, porous implants have a vast surface area that is highly prone to corrosion due to galvanic and crevice corrosion and leaking substantial amounts of ions that cause severe postoperative complications such as osteolysis, allergenicity, toxicity, and implant failure [103]. Highly porous implants made from Mg and Zn alloys are unsuitable for most cases due to their lower mechanical strength, rapid degradation, and subsequent cytotoxic response [104]. Nonetheless, the controlled presence of limited superficial pores and the addition of Li facilitate osseointegration while avoiding potential adverse effects.

5. Antibacterial mechanism and associated cytotoxic response

5.1. Silver-reinforced alloys

Ag ions, salt, and nanoparticles are well known for corrosion resistance and antibacterial properties. The addition of silver in a degradable Mg and Zn matrix helps to release Ag^+ ions that can attach with the thiol (-SH) protein enzyme of bacteria and break the hydrogen-sulfur bonding. In consequence, the bacteria cell died. Ag^+ ions create a chain reaction as ions can be free after the cell destruction and attack another bacteria cell. The killing mechanism of Ag^+ ions encompasses the inhibition of the replication of bacteria by attaching to their DNA and RNA [105] or changing the inherent structure by creating a bond with the proteins [106]. Eq. (16) and Fig. 3 have demonstrated the antibacterial action of Ag^+ ions [85]. Tie et al. [107] tested Mg-xAg (x = 2,4,6) alloys and observed that the initial in-vivo degraded product of Ag is AgCl, which further releases Ag^+ ions that kill above 90% of *S. aureus* and *S. epidermidis* bacteria. However, the formation of AgCl reduces the free $Ag^{+,}$ which reduces cytotoxicity [108].

$$2AgCl \rightleftharpoons 2Ag^+ + 2Cl^- \tag{15}$$

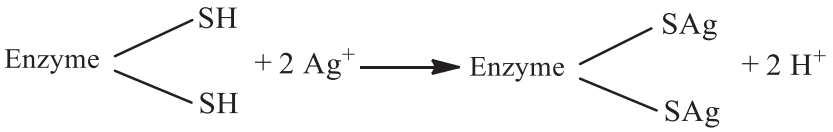

(16)

Qu et al. [109] investigated the antibacterial, antiosteolysis, and internal fixation performance of Zn-xAg (x = 0, 0.5, 1, 2) alloys on a rat femur, mouse cranial, and rabbit femoral condyle. Zn-2Ag prevented staphylococci growth, responsible for rabbit bone loss, MRSA, and MRSE. It also suppressed the activated osteoclast and blocked mouse cranial osteolysis. Fig. 4 illustrates the micro-galvanic corrosion of Zn-4Ag resulting in a selective dissolution of Zn, and Zn_3Ag enriched surface has been revealed, thus initiating cytotoxic effects and

Please cite this article as: C.A. Shahed, F. Ahmad, E. Günister et al., Antibacterial mechanism with consequent cytotoxicity of different reinforcements in biodegradable magnesium and zinc alloys: A review, Journal of Magnesium and Alloys, https://doi.org/10.1016/j.jma.2023.08.018

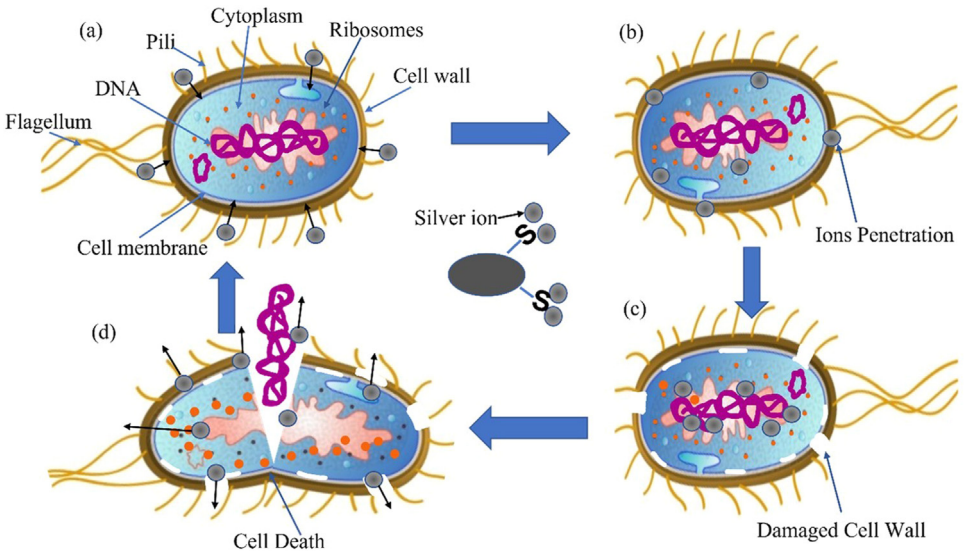

Fig. 3. A schematic diagram of Ag ions' antibacterial action; (modified and redrawn) [85].

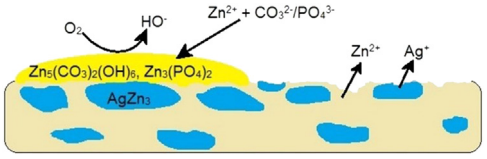

Fig. 4. Selective dissolution of Zn and Ag from Zn_4Ag alloy surrounded by second phase Zn_3Ag. Increased corrosion releases more Zn^{2+} and Ag^{+} ions induced cytotoxicity; (modified and redrawn) [110].

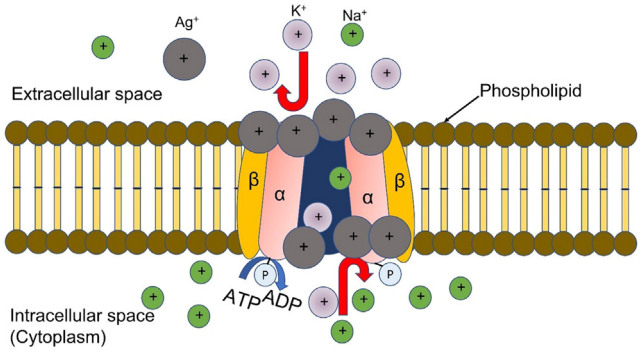

Fig. 5. Schematic diagram of Na-K-ATPase into the cell membrane. The Ag+ ions have inhibited ionic transport through α subunits, causing cell death.

increasing necrosis [110]. Alloys with more than 1 wt% Ag significantly decrease cell proliferation and cell adhesion due to the rise of pH values [111].

Liu et al. [112] prepared Mg-6Ag and Mg-8Ag alloys and evaluated the cytocompatibility and antibacterial performance via biofilm culture. They found excellent antibacterial properties compared to the Ti control group. For pure Mg, the bacteria viability was around 50%, where the Mg-6Ag and Mg-8Ag showed 18.64% and 14.75%, respectively. Similar results were found for the biofilm culture, although the T4-treated alloy performed less microbicidal than the extruded counterparts due to slow degradation. Besides, Mg-6Ag and Mg-8Ag could not reach 75% cell viability, indicating high cytotoxicity. After diluting the extracts five times, the extruded Mg-6Ag and T4-treated Mg-6Ag samples surpassed 80% efficacy, while only the T4-treated Mg-8Ag sample achieved the same threshold. Dai et al. [113] developed RE element yttrium (Y) reinforced Mg-Ag alloy to improve mechanical and antibacterial activity. After 24h of testing, extruded Mg-4Y-Ag showed 92.93% antibacterial inhibition for *S. aureus* with no cytotoxicity (L929, fibroblast).

Ag nanoparticles (NPs) are active antibacterial elements that can prevent bacterial adhesion on the implant surface, penetrate the cell membrane of bacteria, release ROS, and prevent DNA replication [114]. AgNPs ranging from 3 nm to 9 nm have shown the most effective antibacterial properties for gram-negative bacteria [115], although a relatively larger 40 nm NP Ag is effective for gram-positive bacteria [116]. A similar result has been found by Florea et al. [117] developed AgNPs doped $Mg_3(PO)_4$ coating deposited on the orthopedic implant by using the matrix-assisted pulsed laser evaporation (MAPLE) technique. They observed bacteria cell count after 24h and 48h were $\sim 1 \times 10^{11}$ and $\sim 1 \times 10^{13}$ CFU/mL, respectively. The inhibited cell number was $\sim 1 \times 10^{5}$ CFU/mL for an uncoated and coated sample. AgNPs are not as effective (up to 44.3%) as gold NPs (up to 93.6%) against *P. aeruginosa and S. aureus* biofilm and *Laccaria fraternal* fungal strain [118,119]. Oppositely, different hydroxides, homogeneous and non-homogeneous Ag_2O and AgO, give oxidative stress on the cell membrane, DNA of the cells, and proteins by forming ROS. Besides, it restricts the activities of sodium and potassium adenosine-triphosphatase (Na^+, K^+-ATPase), thus hampering the flow of Na^+, K^+ and killing animal cells. Fig. 5 illustrates the inhibition effects of Ag^+ for sodium-potassium pump.

The reason behind the severe cytotoxic outcome of Ag+ is not well defined. Researchers [120] correlate silver cytotoxic-

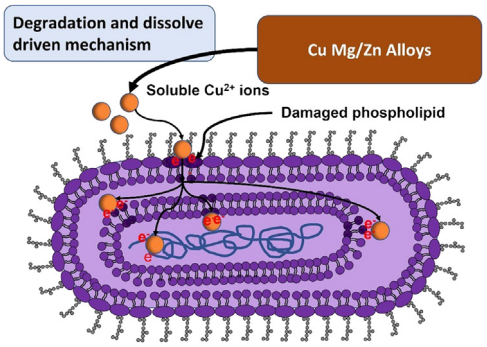

Fig. 6. Schematic diagram of Cu^{2+} ions antibacterial action in *E-coli.* Degraded implants release soluble Cu ions, which extract electrons from the cell membrane and damage the central nucleoid [125].

ity with particle size and ion concentration as 10 nm AgNPs are significantly cytotoxic than 100 nm particles for human lung cells. The underlying cause for such an outcome lies in the antibacterial properties of Ag^{+}. The human cell's component, including cytoplasm, mitochondria, and the nucleus, contains the thiol group, which plays a vital role in cellular function, including protein folding, enzymatic reaction, and antioxidant defense mechanism [121–123]. Similar to antibacterial action, Ag+ creates a bond with the thiol group and hampers the normal functionality of body cells. Accumulation of AgNPs might block the necessary transportation of Na^{+} and K^{+} electrolytes into the body cell, causing cellular swelling and cell death. Therefore, large AgNPs and lower ion concentrations show acceptable cytotoxicity.

5.2. Copper-reinforced alloys

Cu has antibacterial and anti-inflammatory properties, and it also prevents the proliferation of malignant cells [124]. Cu substrates in the suspension are attracted to the cell membrane due to the electrostatic force and soluble Cu^{2+} ions internalized inside the cell [125]. These ions usually do not damage the DNA of bacteria; instead, the strong ability of Cu^{2+}ions extract electrons from the cell membrane of bacteria, thereby pulling out the cytoplasm and oxidizing the nucleus [126]. Fig. 6 illustrates the Cu^{2+} ion's antibacterial action. The OH^{-} in the basic solution could break the protein's ionic bonds, alter the DNA structure, and inhibit its replication [127]. Cu-nanoparticles are also bactericidal elements with various cell-killing mechanisms, including lipid peroxidation, ROS release, DNA degradation, and nucleus oxidation [128].

Li et al. [129] formulated three Mg-xCu, (x = 0.05, 0.1, 0.25) alloys to assess the antibacterial activities of an MRSA. The in vitro antibacterial testing was performed on *E. coli, S. epidermidis*, and MRSA and found a few bacteria colonies on the Mg-0.25Cu glass plate. Similarly, the Mg-0.25Cu alloy showed considerably lower osteomyelitis (swelling in the bone) with the usual surface morphology for in-vivo testing on rabbits' tibia. Alloy with higher Cu content effectively inhibits bacterial colonies. Fig. 7 illustrates the bacteriostatic ability of Zn-xCu, (x = 0, 0.5, 1, 2) alloys. Four types of bacteria, *S. aureus, S. epidermidis*, MRSA, and MRSE were cultured on the sample's surface and counted using plating gradient dilution techniques. Results showed (Fig. 7a) that Zn-2Cu completely eradicated all types of bacteria. Also, distorted, shrunk, and raptured bacteria cell morphology was observed (Fig. 7b) on Zn-Cu alloys [130]. Tong et al. [131] observed that the threshold tolerance limit for a specific cell is related to cytotoxicity. The order for toxicity is Zn < Pb < Cu, where heavy metal like Cu has a greater toxic effect than Zn [132].

The degradation rate of Cu-Zn/Mg alloy increases with the increase of Cu content [129,130]. In Zn-Cu alloys, Zn of the adjacent location of the dendritic structure ($CuZn_5$) degrades drastically due to the galvanic corrosion effect and induces cytotoxicity [130]. A similar result has been found by Tong et al. [133], where untreated and heat-treated Zn-Cu foams were tested. Heat treatment reduced the Cu^{2+} concentration from 34 ± 2 ng/mL to 16 ± 2 ng/mL, and cell viability improved from 26 ± 2% to 82 ± 2% after one day of immersion at 50% extracts. Only more than 90% cell viability can be achieved for Cu ions at 4.2 μg/L. Surprisingly, Bao et al. [134] found almost no cytotoxicity for Zn-1Cu alloys (Zn ion concentration 17.7 ± 1.8 μg/mL and Cu ion concentration 0.0214±0.004 μg/mL) for intrauterine devices, although endometrium inflammation observed for excessive release of Cu^{2+} ions from pure Cu implant (130.1 ± 5.6 μg/mL). Another study showed the cytotoxicity of Zn-4Cu pure extracts to EA. Hy926 cells only had a 20% cell viability, while the diluted extracts (up to 50%) showed almost 100% cell viability [68]. Fig. 8 shows the Sprague-Dawley rat's damaged endometrial stromal cell structure due to the Zn-Cu cytotoxicity.

The Cu substance is also used in coating content to improve corrosion resistance and antibacterial activity. Chen et al. [135] developed Mg-2Zn-1Gd-0.5Zr alloy and coated with Cu-MAO coating (1 g/L HA, 1 g/L CuO nanopowders, 8 g/L potassium fluoride (KF), and 3 g/L $(NaPO_3)_6$). The corrosion rate was 0.16 mm/yr and showed no cytotoxicity. Moreover, the bacteria-killing rate reached 95% after 12hr. A recently developed metal-organic zeolitic imidazolate framework (ZIF) can be used as an excellent platform to release the desired ions in a controlled fashion. This can be achieved due to the high surface area, ease of dope, adjustable pores, good biocompatibility, thermal stability, and commercial availability [136,137]. The antibacterial property depends on the oxide state of copper. Cu_2O kills bacteria by damaging fumarase due to its low molecular concentration. CuO can convert to Cu_2O in an anaerobic environment, creating severe toxicity to *E.coli* compared to CuO. On the other hand, CuO produces a significant amount of ROS to perform bactericidal/ bacteriostatic activities [138].

Ling et al. [139] Tested the biocompatibility and antibacterial properties of copper-doped ZIF-8/Hydroxyapatite composite coated on AZ31 alloy. They prepared three samples with 15%, 30%, and 45% copper content and found 99.99% effective against bacteria, and the CFU/mL decreased from 10^9 to 10^3 due to the presence of Cu^{2+} and Zn^{2+}ions.

Please cite this article as: C.A. Shahed, F. Ahmad, E. Günister et al., Antibacterial mechanism with consequent cytotoxicity of different reinforcements in biodegradable magnesium and zinc alloys: A review, Journal of Magnesium and Alloys, https://doi.org/10.1016/j.jma.2023.08.018

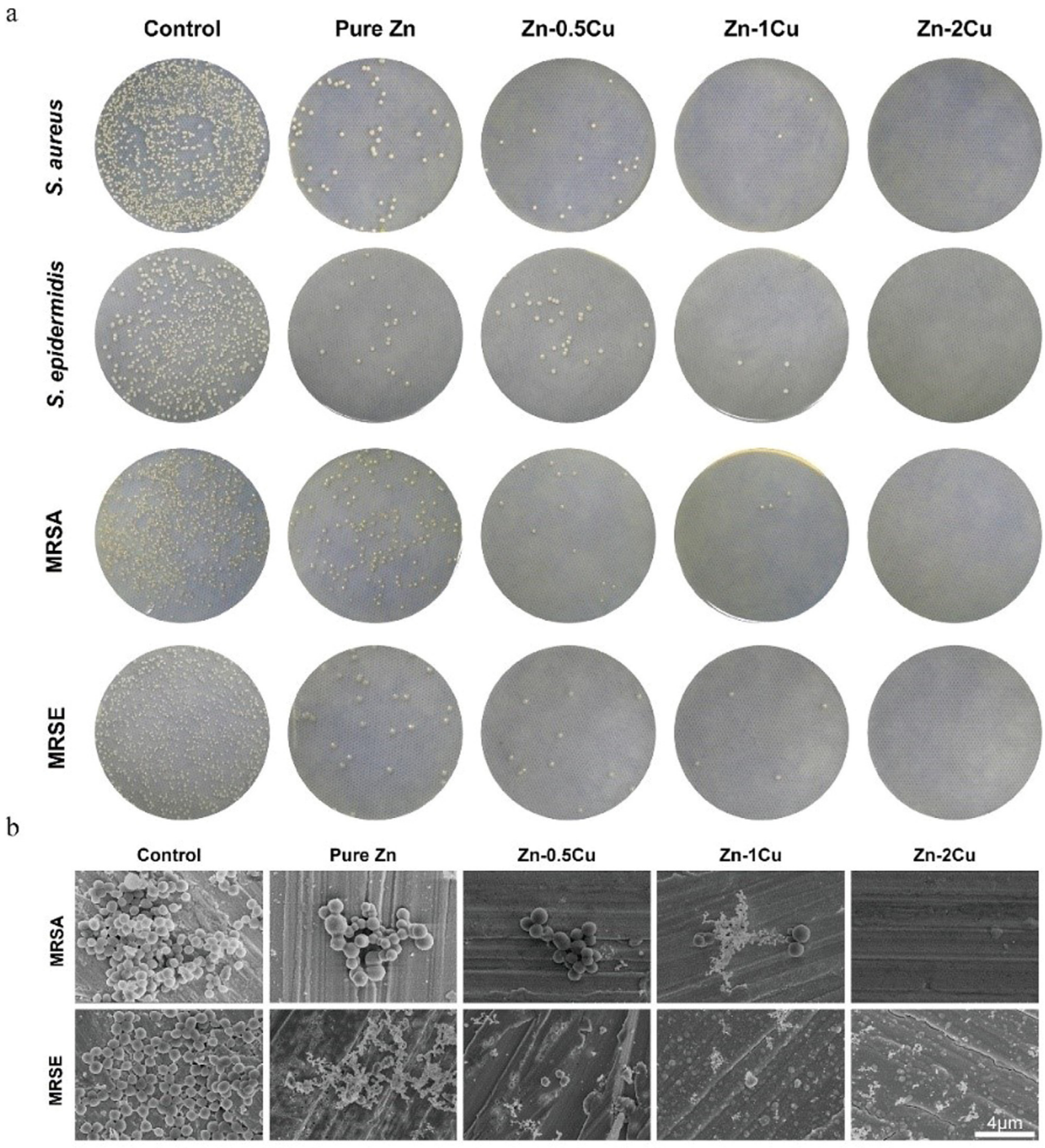

Fig. 7. Images represent (a) Bacteria growth after 24 h on the surface of samples, including pure Ti as a control. (b) Cell morphologies of MRSA and MRSE strains on the surface of the sample (reproduced with permission) [130].

MC3T3-E1 cells were cultured and found above 80% cell viability for all three Cu-doped-ZIF-8 samples. The ion release rate was stable after seven days of immersion in the SBF, and the highest release was 8881.56 μg/L observed from 45% Cu-ZIF-8/HA, which was considered in the low concentration range. This low ion release was achieved due to the dodecahedron structure of Cu-doped ZIF-8. Therefore, it can be concluded that excessive Cu ions have a detrimental effect, while a small quantity of Cu ions enhances cytocompatibility. The electronegativity of Cu (1.9) is higher than Zn (1.65) and Mg (1.31); thus, Cu^{2+} shows more cytotoxicity than Zn^{2+} and Mg^{2+}.

5.3. Magnesium/zinc reinforced alloys

Both Mg and Zn itself have antimicrobial properties with good degradation rates. Lin et al. [140] cultured *E.coli* and *S. aureus* on 316LSS, pure Zn, and Zn-0.02Mg and found

Please cite this article as: C.A. Shahed, F. Ahmad, E. Günister et al., Antibacterial mechanism with consequent cytotoxicity of different reinforcements in biodegradable magnesium and zinc alloys: A review, Journal of Magnesium and Alloys, https://doi.org/10.1016/j.jma.2023.08.018

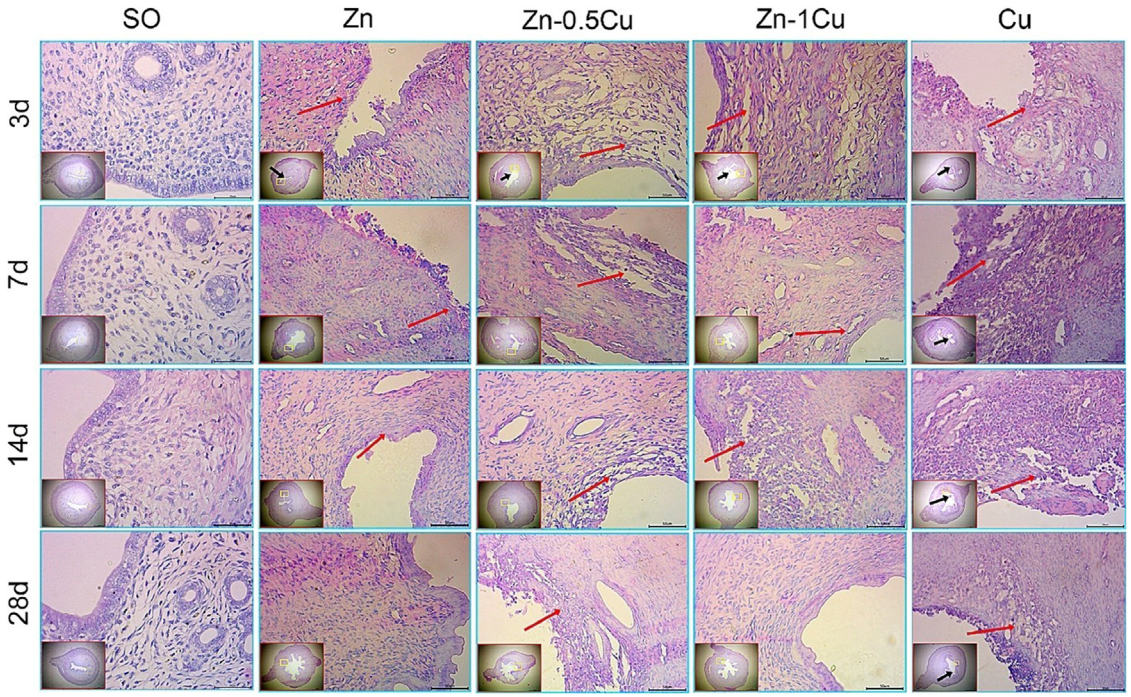

Fig. 8. Histological photographs of Sprague-Dawley rat uterine tissues stained with hematoxylin and eosin. The inset depicts uterine cross sections, and the magnified picture is the square area in the inset. The endometrial structures were disrupted after implantation, as seen by the damaged structure of endometrial stromal cells (red arrows). Zn-1Cu group has moderate tissue responses than other groups, and SO indicates the sham-operated group (reproduced with permission) [134].

that both Zn and Zn-0.02Mg showed good antibacterial properties. However, Zn-Mg alloy cannot suppress *P. Aeruginosa* bacteria biofilm due to its metal-resistant strains capability (MRSC) [141]. These bacteria bear an extracellular polymeric constituent that protects the biofilm by preventing biofilm diffusion [142]. The antibacterial mechanism for Mg^{2+} and Zn^{2+} ions is similar to the Ag^{+} and Cu^{2+} ions. The in-vitro cytotoxic response of undiluted extracts for pure Zn implant is comparable to Zn-3Ag [143]. Zn-3Mg alloy showed significant toxicity on NOHst cells with cell viability of 47% ± 12% after one test day [144]. Cytotoxicity response depends on the cell type; L929 was found more sensitive to Zn ions than U-2 OS for Zn-xMg (x = 0–1.6 wt.%) alloys [145]. The highest safe concentrations are 120 μM and 80 μM, respectively, for Zn-0.8Mg alloy; overall, it shows less cytotoxicity behavior than Zn-3Ag. Fig. 9 depicts the fluorescent photograph of alive MG63 osteoblast cells where cells' morphology was changed above 12.5% extracts (Zn ion concentration 11 mg/L for pure Zn implant) of all compounds. Besides, the 100% Zn extract exhibits more detrimental results than Zn-3Ag. Nonetheless, the in vivo results often do not show such strong cytotoxic effects for Zn implants due to the blood circulation and complex body environment [146].

Zhang et al. [147] compared the antibacterial ability, cytocompatibility, and osteogenicity of ZC21 (Mg-2Zn-0.5Ca) over Mg-4Zn-1Sr (ZSr41) and pure Mg. ZC21 performed better adhesion of bone-marrow-derived mesenchymal stem cells (BMSCs) in both direct and direct exposure cultures. They also cultured the MRSA and found the lowest 1.5×10^5 CFU/mL after 24 h. The degradation rate inside the mouse femoral was also lower than ZSr41, and after 12 weeks of implantation, ZC21 promoted bone growth along with the smallest gap found at the femoral defect. Zou et al. [148] developed Zn-doped montmorillonite (MMT) coatings on AZ31 alloy and tested the antibacterial property of *E. coli* and *S. aureus*. They observed the damaged bacterial cells and leaked out the intracellular substance of the bacteria on the Zn-MMT. Zn-MMT was more effective for gram-positive bacteria as the zone inhibition was 22 mm and 32 mm for *E. coli* and *S. aureus,* respectively. Besides, the cytotoxicity assessment was also favorable for Zn-MMT coatings since the cell viability remains above 75% for MC3T3-E1 after 72 h of culture. Bhatt et al. [149] extracted Zinc acetate dihydrate from the Eucalyptus seed extracts and prepared Mg-doped Zinc oxide to test the antibacterial property. They cultured *E. coli* on an agar plate, observed 22.66 mm and 17.66 mm inhibition zone (IHZ) for the 75% Mg-ZnO nanoparticles and ZnO nanoparticles, respectively, and concluded that the combined effect of Mg and Zn ions inhibits the bacteria growth.

Gram-negative and gram-positive bacteria mostly have mesh-like peptidoglycan around their cytoplasmic membrane with a thickness of 20–80 nm and 2–3 nm, respectively [150]. ZnO NPs with an average particle size of 25.7 nm can easily interact with gram-positive bacteria and damage the cell membrane. Dopants like Co can further reduce the particle size (20.5 nm) to improve the binding strength, produce more ROS components, and increase the bactericidal activity [151]. Particles size less than 10 nm can directly pierce the bac-

Please cite this article as: C.A. Shahed, F. Ahmad, E. Günister et al., Antibacterial mechanism with consequent cytotoxicity of different reinforcements in biodegradable magnesium and zinc alloys: A review, Journal of Magnesium and Alloys, https://doi.org/10.1016/j.jma.2023.08.018

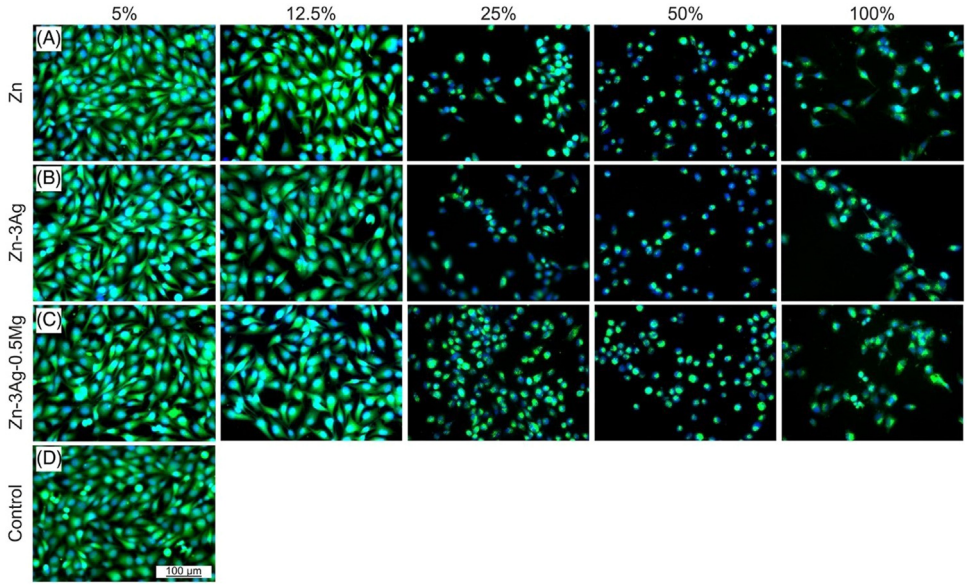

Fig. 9. Fluorescent images of MG-63 Osteoblast cell stained with calcein-DAPI after 1 day of indirect cell culture for pure (A) Zn, (B) Zn-3Ag, (C) Zn-3Ag-0.5Mg. The scale bar is 100 µm for all images. (Reuse permission: open access) [143].

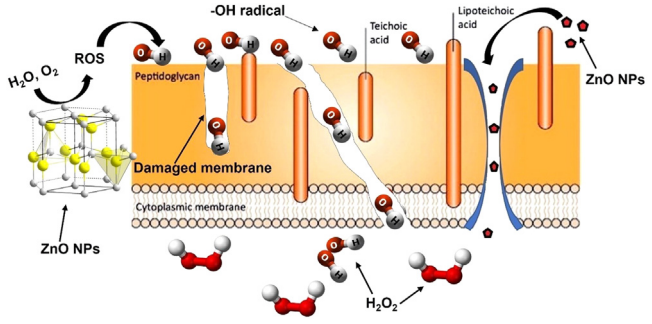

Fig. 10. Gram-positive bacterial cell wall surrounds peptidoglycan containing teichoic and lipoteichoic acid. -OH radicals damage cell membranes and create a pathway to penetrate H_2O_2 and destroy DNA protein [150,153].

terium cell membrane [152]. ROS is the common antibacterial technique for ZnO NPs where hydroxyl radical (-OH), superoxide (O^{2-}), and H_2O_2 (hydrogen peroxide) destroy the bacteria cell membrane and DNA protein. Fig. 10 gives an illustration of the antibacterial actions of ZnO NPs. These bactericidal techniques are also valid for CuO, TiO_2, Au_2O_3, and Ag_2O NPs [153].

Based on the preceding discussion, it is evident that the synergistic action of Mg and Zn can effectively kill bacteria except for MRSC bacteria. Additionally, the findings of 10 nm ZnO particles' ability to pierce bacterium cells support the cytotoxic effects observed in AgNPs. It indicates that particles roughly 10 nm in size could possess detrimental effects on body cells.

5.4. Gallium-reinforced alloys

Gallium (III) is well known as a chemotherapeutic agent, and its antibacterial properties depend on the chemical mimicry with iron (III) [154]. Fe^{3+} is an essential ion for DNA replication, anti-oxidative stress, and electron transfer of bacteria. Due to the similarity of Fe^{3+} and Ga^{3+}, the iron acquisition pathway of bacteria can be used for Ga transport and can inhibit replication by creating a bond with the bacteria envelope and preventing Fe metabolism [85,155]. Excluding that, Ga hampers the functional activity of deoxyribonucleotide reductase, an iron-containing enzyme, reducing the chance of forming biofilms [156]. Recent studies found that Ga ions can inhibit aerobic bacteria more effectively than anaerobic bacteria, indicating the ROS association in antibacterial action. Lin et al. developed a partially Ga-coated Zn-based biodegradable micromotor to kill the targeted *Helicobacter pylori* bacteria. The cell viability at 2 mg/mL ion concentration was 85%, indicating minimal cytotoxicity. The propulsion technique of micromotor was involved with the H_2 gas evolution in the acidic environment, although no significant pH change was not observed. Eq. (17) [157] gives the reaction with acid (H^+ ions) and Zn to produce H_2 bubbles. Fig. 11 shows the functionality of Ga/Zn Janus micromotor.

$$Zn(s) + 2H^+ (aq) \rightarrow Zn^{2+} (aq) + H_2 (g) \quad (17)$$

Gao et al. [158] investigated the combined effect of Ga^{3+} and Sr^{2+} on *S. aureus* and *E. coli* in in-vitro and in-vivo conditions with cytotoxicity analysis. Although the in-vitro cytotoxicity report for human MSCs was unfavorable, with 50% dead cells, the in-vivo (mouse femur implant) antibacterial and biocompatible results were convincing due to the dynamic flow of ions inside the body. At the beginning of immersion, cytotoxicity could be observed due to the massive Mg^{2+} release; soon, the ion release rate reached a toxic level of 1000 ppb/h for Ga^{3+} after 48–72 h. Vukomanovic et al. [159] tested an osteogenic effect on human MSCs and antibacterial activity by developing a multi-doped apatite with Mg^{2+}, Sr^{2+}, Zn^{2+}, and Ga^{3+} ions. Due to the good synergistic effect, the inhibition of bacteria growth and prolonged

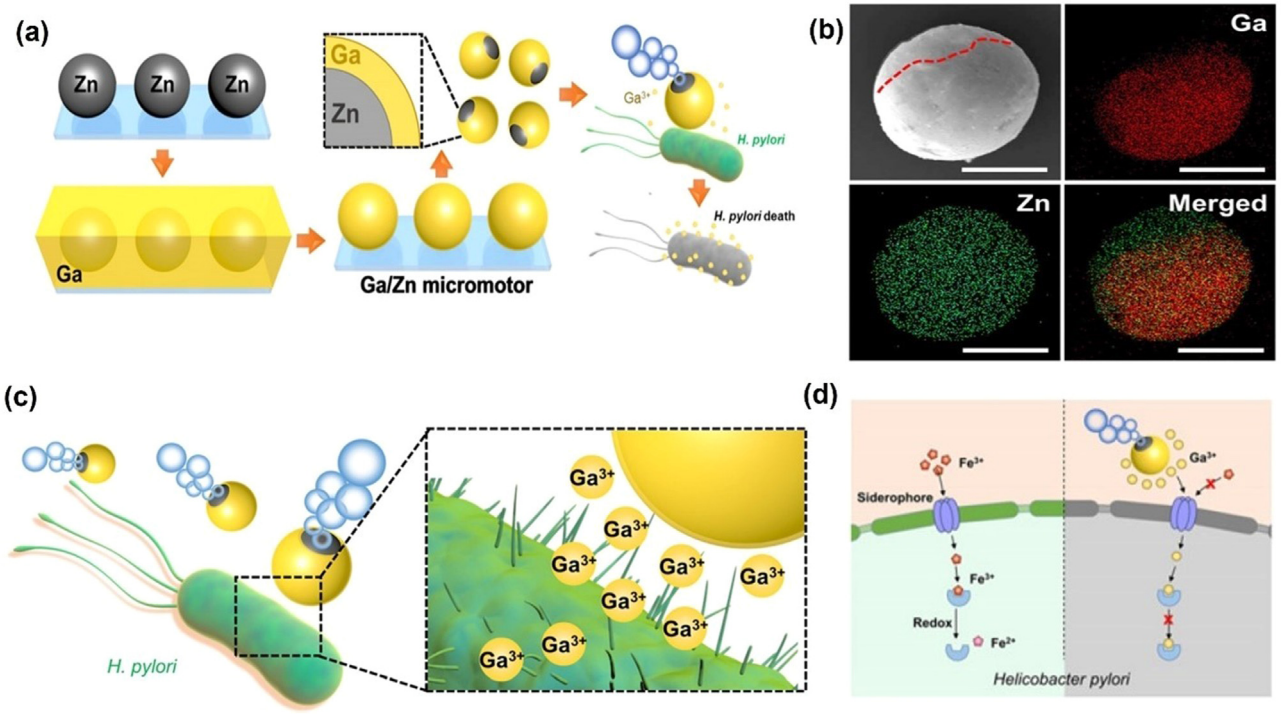

Fig. 11. Schematic diagram of (a) Ga/Zn Janus micromotor's fabrication and antibacterial action, (b) EDX mapping, (c) Ga^{3+} ion release, and (d) Ga^{3+} ion prevents Fe^{3+} penetration and binds with the receptor (Reproduced with permission) [157].

antibacterial protection were achieved. Compared to single-doped apatite, ions release for multi-doped apatite was inferior; however, the antimicrobial effects were the same, with satisfactory cell viability results of less than 20 LDH (Lactate dehydrogenase) value for human MSCs cells.

Ga^{3+} can be evenly embedded in chitosan using in-situ precipitation by using chitosan's chelation capacity. The chitosan-Ga ion complex successfully inhibited more than 90% of *E. coli* bacteria compared to pure chitosan implant after 24 h [160]. Conversely, cytotoxicity was observed on MG63 osteoblast cells for high Ga^{3+} to chitosan ratio of 1:16, 1:8, and 1:4 with cell viability of around 63 ± 2%. The cytotoxicity is dose-dependent for both Ga^{3+} and chitosan [161]. Therefore, the synergistic effect reinforced the cytotoxic effect. Song et al. [162] developed Ga-Sr-PO_4 coating and found that Ga-Sr-PO_4 coating on Mg protects the nucleus damage of osteoblast cells. The dead cell count for pure Mg was 60%, whereas the dead cell count for coated Mg was 16% only. Similar success was observed in antibacterial performance, where the inhibition rate was 78% and 57% after three days of incubation for *P. aeruginosa* and *E. coli*, respectively.

Ga has excellent effects on bone growth affirmatively by reducing the loss of bone site calcium. Ga salt can be used for bone regeneration and osteoporosis-related diseases [163]. It may be responsible for accumulating hydroxyapatite (HA) and phosphorus in the bone, as they are also essential components of bone. Also, the Ga-doped HA (HAp(Ga)) has antibacterial properties against P. aeruginosa, *E. coli,* and *S. epidermidis.* Moreover, arginine functionalized gold with HA (Au/Arg@HAp(Ga)) exhibited more than ten times superior antibacterial properties than those without Ga counterparts [164]. The 0.1 mg/mL concentration inhibited bacteria growth over 1 mg/mL (Au/Arg@HAp) (without Ga). A comparable result was found while testing Ga-bioactive glass, ($0.42SiO_2$- $0.10Na_2O$-0.08CaO-(0.40-x)ZnO-(x)Ga_2O_3) [165]. A comparison was made by Sara et al. [166] between Ga- mesoporous bioactive glasses (MBGs) and non-Ga-MBGs. Researchers concluded that 3% Ga-MBG showed better antibacterial properties, achieving a 99% antibacterial rate against E. coli and S. aureus, surpassing 1% and 2% Ga-MBG counterparts. The increased amount of Ga_2O_3 content releases more Ga^{3+} ions, resulting in higher pH, which might be the mechanism of killing bacteria. On the contrary, low (1%) Ga_2O_3 contained MBG showed excellent cytocompatibility and hemostatic properties and helped to stop bleeding by platelet adhesion. Overall, the antibacterial mechanism for Ga^{3+} is relatively safe as it blocks the nutrients of the bacteria. Since ferric ions are critical components of blood hemoglobin and are responsible for oxygen transportation, iron deficiency can lead to anemia and internal bleeding [167]. This phenomenon can be correlated with the above findings, as the accumulation of Ga^{3+} might hamper the regular balance of Fe^{3+}. Nevertheless, a detailed study is still necessary in this field for better understanding.

5.5. Lithium-reinforced alloys

Recent studies have found mild antibacterial properties in Li. Like Ag^+ ions, Li^+ ions attach with the thiol group of

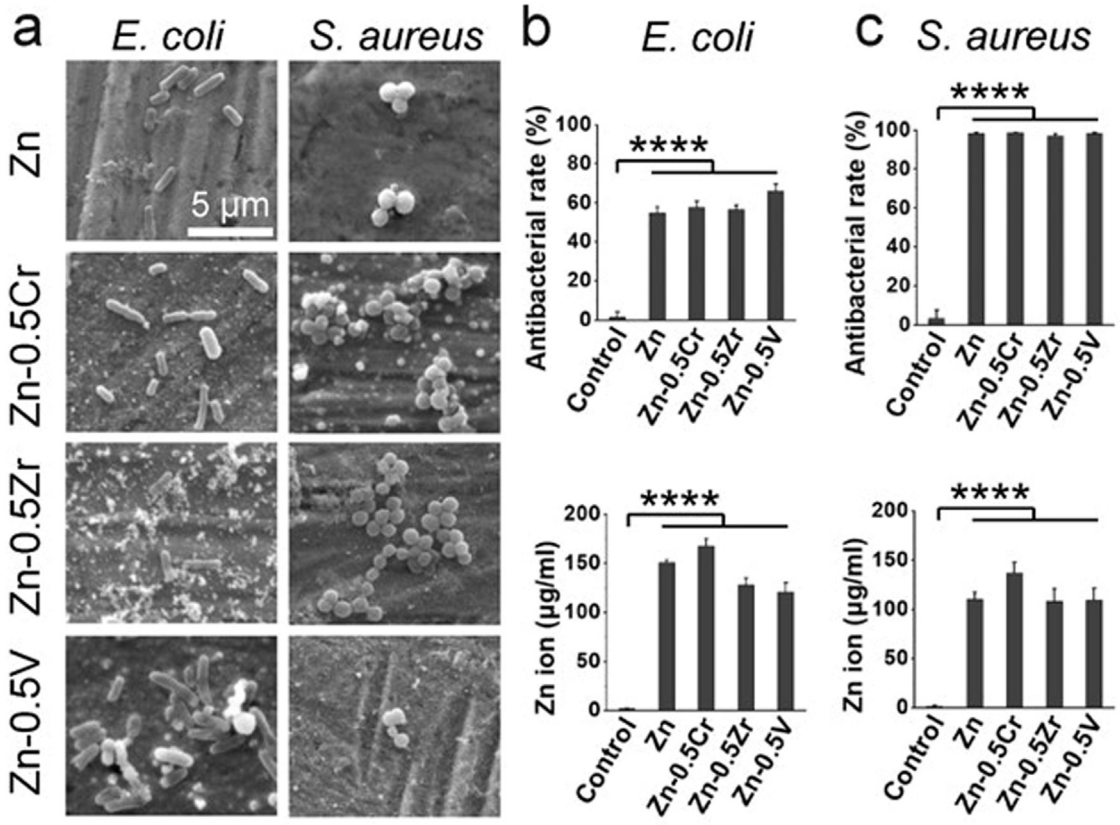

Fig. 12. Antibacterial operation with *E. coli* and *S. aureus* after 24 h. on pure Zn and Zn-0.5x (x = *V*, Zr, Cr) alloy surfaces. (a) SEM images of bacterial adhesion. Antibacterial rates and corresponding Zn ion concentrations in the culture medium after culture with (b) *E. coli* and (c) *S. aureus* (Reuse permission: open access) [173].

the bacteria and damage the cell envelope [168–170]. If Li is doped with metal oxides, it helps to produce more O^{2-}. The generated O^{2-} dissolves in water and produces hydrogen peroxide, followed by the generation of ·OH by oxyhemoglobin and methemoglobin, thus causing oxidative damage to the protein and DNA of bacteria [169,170]. Simultaneously, Zn-modulated Li caused hepatotoxicity in rats, although Zn shows hepatoprotective efficacy [171]. Researchers anticipated that due to the direct effect of Li, lipids and proteins degenerated rapidly, affecting rats' livers. Hence, Li degradation needs to be controlled to dissolve cytotoxicity issues. A non-porous and polished surface could prevent degradation, as polished surfaces showed four times less degradation than porous surfaces [172].

5.6. Other transitional metals reinforced alloys and coatings

Other than Ag, Ga, and Cu, some transitional materials, e.g., V, Cr, and Zr, are used nowadays with Zn to enhance mechanical properties and inhibit bacteria. Zn-0.5Cr showed the highest five-fold degradation than others in rat's femur, and all the Zn alloys showed a good bone-tissue response. After three months of implantation, the tissue reached the osteoid to the bone [173]. Tong et al. [174] developed a dysprosium (Dy) alloyed Zn composite and found improved cell viability and antibacterial properties. Fine-grained hot-rolled samples showed a greater degradation rate. Fig. 12 shows the Zn ion release (μg/ml) and antibacterial rate for Cr, Zr, and V alloys. All the alloys have demonstrated at least 50% efficacy for *E. coli* and 99% for *S. aureus*. The antibacterial property correlates with the release of Zn ions. Nevertheless, Zn-0.5 V alloy has performed better than expected. Zn and V might have a synergic effect to do a score of bacteria-killing more than 60%.

Sol-gel, a "green" process, is a cost-effective way of high-quality coating on Mg and Mg-alloys to achieve targeted properties like cytocompatibility, osteogenic, and antibacterial properties. HA-coated Mg shows good biocompatibility with sacrificed corrosion resistance properties in the aqueous medium. Substances like TiO_2 nanoparticles, silver and silver compounds like $Ag/AgBr/TiO_2$ and $AgTi_2(PO_4)_3$ have bactericidal and bacteriostatic ability for both gram-positive and gram-negative bacteria, respectively, although they also have cytotoxic properties [175]. Sol-gel TiO_2-coated HA-coated Mg alloy improved corrosion behavior by creating a thin layer on the porous HA-Mg surface. TiO_2 generates ROS, owing to its strong oxidizing capabilities, to kill bacteria effectively [176]. ROS can be produced by a layered double hydroxide (LDH), and black Mn-comprised LDH nanosheet containing Mg alloy can be used to treat osteosarcoma bone cancer and bone regeneration. Mn-contained LDH has photothermal properties and Fenton-like catalysis that can generate heat

(vibration energy) and in-situ hydroxyl radicals (·OH), respectively, to kill targeted cells and in-site bacteria [177]. A similar approach was taken by Zhang et al. [178], where they developed sodium copper chlorophyllin ($C_{34}H_{31}CuN_4Na_3O_6$)-CaP layer-by-layer (LbL) coating on hydroxylated AZ31. The $C_{34}H_{31}CuN_4Na_3O_6$ has a photodynamic and photothermal therapy effect that is effective in a broad spectrum of bacteria. Cui et al. [179] coated an antibacterial coating consisting of chitosan and deoxyribonucleic acid (DNA) on AZ31 alloys by adopting alternating LbL assembly with $Mg(OH)_2$ inner degradation protection layer. Chitosan has a contact-killing antibacterial property and hydrophilic nature that ameliorates cell proliferation and adhesion. DNA is a functional polymer that works with Ca^{2+} ions and helps biomineralization [180]. Graphene oxide and HA coating were also applied on the $Mg(OH)_2$ inner layer to enhance osteogenic differentiation without hampering the antibacterial property of $Mg(OH)_2$ [181]. Authors cultured mouse preosteoblasts cell, MC3T3-E1, in an in-vitro condition and found prominent cell growth with cytoplasmic and pseudopodia propagation. Table 1 summarizes the effect of degradation rate and bactericidal ions concentration on antibacterial performance and cell viability.

6. Critical analysis and future prospect

It is evident from the above study that bactericidal performance depends on the concentration of metal ions released during biodegradation and their oxidation number. Increased ionic release changes the localized pH level and affects the antibacterial performance. Not all the metal ions react in the same way with water. Metals from Group 1 and Group 2 in the periodic table (e.g., Li^+, Sr^{2+}, Na^+, Mg^{2+}) perform basic hydrolysis and form hydroxyl radicals (OH-), thus increasing pH [193]. Several metal ions (e,g., Al^{3+}, Zn^{2+}, Cu^{2+}, Ga^{3+}, and Cr^{3+}) show amphoteric behavior and produce OH- when they react with water [194]. Bacteria have an ideal pH state to perform enzyme functional activity and metabolism. Imbalance pH kills bacteria by damaging cell membranes by altering protein structure and making it more permeable, disrupting cellular processes, and inhibiting bacterial growth. Higher pH reduces nutrient availability and blocks metabolic pathways, including ATP and protein synthesis, electron transport chain, and enzyme inactivation [195,196].

The DNA and RNA of bacteria are composed of nucleotides containing a sugar molecule, a nitrogenous base, and a phosphate group. Four different nitrogenous bases have been found in DNA and RNA, and hydrogen bonds hold two strands of DNA together [197]. Li, Al, and Mg metal ions with solid antibacterial properties exhibit strong reactions with nitrogen, hydrogen, and oxygen, altering the structure of sugar molecules and a nitrogenous base. From the metal-phosphate solvation study [198], the energy for solvation complexes of a different phosphate group in a nucleic acid environment is usually lower, and it varies as $Mn^{2+} > Mg^{2+} > Ca^{2+} > Li^+ > Na^+ > K^+$. Lower solvation complex energy indicates stronger solute-solvent molecular attachment and higher stability. These bonding lead to DNA and RNA breakage and killing bacteria. Although Ag^+ shows a slow reaction with a phosphate group, it condenses DNA molecules and damages their replication ability [105]. Also, a link to metal type, cation number, and antibacterial properties has been observed. Type-I metal (formed only one type of cation) showed superior antibacterial properties than type-II metal (formed more than one type of cation) if the highest cation numbers are the same for two comparable metals, and the cation number has the opposite relation with the antibacterial properties. Although Cu and Ag belong to the same Group 11 in the periodic table and Cu, Ag, and Zn all are transitional metals, Ag and Zn are type I metal with +1 and +2 cation number, respectively. On the other hand, Cu is a type II metal with +1 and +2 cation numbers. According to this hypothesis, Ag and Zn should have more antibacterial efficacy than Cu. Durdu et al. [199] validated this hypothesis by concluding that Ag performed most effectively, while Zn showed better efficiency than Cu against *S. aureus* and *E. Coli.* Another study was performed by Sun et al. [200], taking into consideration Ag (I), Cu (II), Zinc (II), and Ga (III). The results indicated that the antibacterial effectiveness followed the order: Ag > Zn > Cu > Ga, consistent with the predictions of the hypothetical model. Therefore, it is evident that metals with +1 and +2 oxidation numbers show relatively strong antibacterial properties than +3. However, the physiological environment is highly complex, and different microbial respond differently; thus, more studies need to be done to establish the hypothesis.

A controlled corrosion rate and hybrid reinforcement approach could prevent a particular ion redundancy and minimize cytotoxicity. Reactive metal reinforcements can produce ROS products and raise WCA, thereby controlling the degradation rate. Cu-reinforced alloys look promising for MRSC bacteria; however, Ga-reinforced alloys look safer among other implants. As the cytotoxic response varies depending on the cell type, implant materials selection should be subjective according to the application. Nanoparticles might have detrimental effects due to the high surface area and accumulation of debris at the implant site. A thorough in-vivo comparison between ion concentration and nanoparticles of the same metal is essential.

The target killing of bacteria using photodynamic and photothermal effects can be competent if the generation of ROS can be controlled, although most of the carbon-based photothermal elements cause genotoxicity and lipid peroxidation. Moreover, it is only effective on superficial surface conditions, mostly right under the skin, as light waves need to penetrate to activate the actions. Therefore, further research can be conducted to develop a nontoxic phototherapeutic agent. Researchers mainly exercised a few common bacteria like *E. coli, S. aureus*, MRSA, *S. epidermidis,* and *P. aeruginosa*. Consequently, a wide range of bacteria is left unobserved, and importantly, the harmonious effects of different bacteria in the same site have not been observed yet. Finally, extensive investigation needs to be done on the same material in various locations inside the living body to identify its antibacterial and cytotoxicity performance since the physiological characteristics vary depending on the body's location.

Please cite this article as: C.A. Shahed, F. Ahmad, E. Günister et al., Antibacterial mechanism with consequent cytotoxicity of different reinforcements in biodegradable magnesium and zinc alloys: A review, Journal of Magnesium and Alloys, https://doi.org/10.1016/j.jma.2023.08.018

Table 1
The list of different biodegradable materials with degradation rate, corresponding bactericidal ion, inhibited bacteria, antibacterial performance, and cell viability.

Alloys	Inhibited microbial	Antibacterial performance	Bactericidal ions and concentration (μg/L)	Degradation rate	Cultured cell; viability; extraction concentration	Incubation period	Ref.
Mg-3.16 Nd-0.18Zn-0.41Zr	MRSA, E. *coli*	Antibac. ratio was 90% and 92.1% for MRSA and *E. coli*	Mg^{2+}= 561 at 50% extract, Zn^{2+}	0.039 ± 0.003 gm/d	MC3T3-E1; 49%; 100% MC3T3-E1; 108%; 50%	7d	[182]
PEO	*E. coli, S. aureus*	Initial CFU=100,000. *Remaining:* *S. aureus*= 105, 75 (no NIR, NIR) *E. coli* =4, 0 (no NIR, NIR)		–	MC3T3-E1; 58%; at 100%	7d	[177]
AZ31-PEO-LDH-$MnCl_2{\cdot}4H_2O$ (6 h)	*E. coli, S. aureus*	Initial CFU=100,000. *Remaining:* *S. aureus*= 1400, 14 (no NIR, NIR) *E. coli* =105, 0 (no NIR, NIR)		–	MC3T3-E1; 78%; at 100%	7d	[177]
AZ31-PEO-LDH-$MnCl_2{\cdot}4H_2O$ (9 h)	*E. coli, S. aureus*	Initial CFU=100,000. *Remaining:* *S. aureus*=17,300, 4 (no NIR, NIR) *E. coli* =280, 0 (no NIR, NIR)		–	MC3T3-E1; 77.5%; at 100%	7d	[177]
Mg-0.8Ca	*E. coli,* *S. aureus*	Antibac. ratio, after 1d 80% (for *S. aureus*) 81% (for *E. coli*)	Mg^{2+}	80% degraded by 4 weeks	MC3T3-E1; 81% (*S. Aureus*), 80% (*E.coli)* bacteria-induced; direct culture	1d	[183]
HA-Mg $(OH)_2$ coated MZ-1.5Ag	*E. coli,* *S. aureus*	Antibac. ratio, after 1d 92% (for *S. aureus*) 90% (for *E. coli*)	Mg^{2+}, ·OH	–	MC3T3-E1; 89% (*S. aureus*) 86% (*E.coli)* bacteria-induced; direct culture	1d	[183]
HA-GO-Mg $(OH)_2$ coated MZ-1.5Ag	*E. coli,* *S. aureus*	Antibac. ratio, after 1d 88% (for *S. aureus*) 86% (for *E. coli*)	Mg2+, ·OH,	50% degraded by 4 weeks	MC3T3-E1; 88% (*S. aureus*) 84% (*E.coli)* bacteria-induced; direct culture	1d	[183]
HA-AZ60	*E. coli,* *S. aureus*	Antibac. ratio: HA-AZ60= 19% and 18% for *S. aureus* and *E. coli,* respectively		HEV 3.56 mL/cm^2	L929; 48%; direct culture	5d	[176]
HA-AZ60-TiO_2 (15 times)		HA-AZ60-TiO_2 (15 times) = 99.8% and 99.5% for *S. aureus* and *E. coli,* respectively		HEV 2.18 mL/cm^2	L929; 83%; direct culture	5d	[176]
Mg-1Al-Cu	*E. coli,* *S. aureus*	IZD (mm) 0.99 (*S. aureus)* *1.38 (E. coli)*	Mg^{2+}=86, Cu^{2+}= 0.33, Al^{2+}	0.042 mm/h (after 10 hr)	hMSCs; 23%; 12 mg/mL	7d	[184]
0.18Gr@Mg-1Al-Cu		4.7 (*S. aureus)* *3.7 (E. coli)*	Mg^{2+}= 72, Cu^{2+}= 0.25, Al^{2+}	0.012 mm/h (after 10 hr)	hMSCs; 35%; 12 mg/mL	7d	[184]
0.5Gr@Mg-1Al-Cu		2.4 (*S. aureus)* *1.4 (E. coli)*	Mg^{2+}=83, Cu^{2+}= 0.18,	0.053 mm/h (after 10 hr)	hMSCs; 62%; 12 mg/mL	7d	[184]
AZ31	–	–	Mg^{2+}= 660	34.2 mm/y (after 90d)	EA.hy926; 82.5%; at 50%	3d	[185]

(*continued on next page*)

Table 1 (*continued*)

Alloys	Inhibited microbial	Antibacterial performance	Bactericidal ions and concentration (μg/L)	Degradation rate	Cultured cell; viability; extraction concentration	Incubation period	Ref.
Mg-APC	–	–	Mg^{2+}= 550	0.80 mm/y (after 90d)	EA.hy926; 98.5%; at 50%	3d	[185]
Thiol-ene-Mg-APC	–	–	Mg^{2+}= 325	0.11 mm/y (after 90d)	EA.hy926; 105%; at 50%	3d	[185]
AZ31-Mg $(OH)_2$	*E. coli*, *S. aureus*	Antibac. ratio for *S. aureus* & *E. coli* =62% & 64%	·OH, Mg^{2+}	HEV= 5.92 ± 0.69 mL cm^{-2}	MC3T3-E1; 93%; at 25%	5d	[179]
AZ31-Mg $(OH)_2$–Chitosan/DNA		Antibac. ratio for *S. aureus* & *E. coli* =93.5% & 95%	·OH, Chitosan, Mg^{2+}	HEV= 3.72 mL cm^{-2}	MC3T3-E1; 91%; at 25%	5d	[179]
MgO NPs	*E. coli, B. subtilis, S. epidermidis, P. aeruginosa*	IZD, *E. coli*= 30 mm; *B. subtilis* = 31 mm; *S. epidermidis* = 20 mm; *P. aeruginosa* = 22 mm	Mg^{2+}, MgO NPs, ROS	–	A-375; 87%, 74%; at 20 μg/ml, 40 μg/ml	1d	[186]
Mg	MRSA	Antibac. ratio ≈52%	Mg^{2+}=2.1 mM	0.63 mg cm^{-2} d^{-1} (in vivo)	BMSCs; 85%	1d	[147]
Mg-2Zn- 0.5Ca	MRSA	≈80%	Cultured with MRSA Mg^{2+}=14 mM; Zn^{2+}= negligible	0.28 mg cm^{-2} d^{-1} (in vivo)	BMSCs; >100%	1d	[147]
Mg-4Zn-Sr	MRSA	≈45%	Cultured with MRSA Mg^{2+}=9.1 mM; Zn^{2+}= negligible	0.37 mg cm^{-2} d^{-1} (in vivo)	BMSCs; >100%	1d	[147]
Zn-3Cu (HR and CR)	*S. aureus*	IZD= 7.68 ± 0.43 mm	Cu^{2+}= 33.2, Zn^{2+}= 36.8	311 ± 9 μm/y (after 90d)	MG-63; 92.8%; at 25%	3d	[187]
Zn-3Cu-0.2Ti (HR and CR)	*S. aureus*	IZD= 7.11 ± 0.32 mm	Cu^{2+}=32.9, Zn^{2+}=35.6, Ti^{4+}=0.9	299 ± 11 μm/y (after 90d)	MG-63; 86.4%; at 25%	3d	[187]
Zn–1Cu–0.1Ti (HR and CR)	*S. aureus*	IZD= 6.99 ± 0.33 mm	Cu^{2+}=14.6, Zn^{2+}=34.8, Ti^{4+}=0.3	32 ± 11 μm/y (after 30d)	MG-63; >83%; at 25%	5d	[188]
Zn-0.8Mn	*E. coli*	Antibac. ratio 81.3 ± 8.3%	Zn^{2+}= 189.5 μM	101± 9 μm/ yr	L929; 95%; at 40%	2d	[189]
Zn-0.8Mn-0.4 Cu	*E. coli*	Antibac. ratio 91.8 ± 2.5%	Cu^{2+}=0.2 μM, Zn^{2+}=127.8 μM	133± 15 μm/ yr	L929; 97%; at 40%	2d	[189]
Zn-0.8Mn-0.4 Ag	*E. coli*	Antibac. ratio 93.7 ± 1.8%	Cu^{2+}=, Zn^{2+}=187.8 μM, Ag= negligible	168± 21 μm/ yr	L929; 78%; at 40%	2d	[189]
Zn-Mg_2Ge	–	–	Zn^{2+}=32, Mg^{2+}=4, Ge^{4+} =6	51.1 ± 2.0 μm/ yr (after 30d)	MG63; 89%; at 25%	3d	[190]
Zn-3Mg_2Ge	–	–	Zn^{2+}=37, Mg^{2+}=13, Ge^{4+} =23	68.4 ± 2.7 μm/ yr (after 30d)	MG63; 85%; at 25% EC	3d	[190]
Zn-5Mg_2Ge	–	–	Zn^{2+}=40, Mg^{2+}=30, Ge^{4+} =38	76.6 ± 2.8 μm/ yr (after 30d)	MG63; 79%; at 25%	3d	[190]

(*continued on next page*)

Table 1 (*continued*)

Alloys	Inhibited microbial	Antibacterial performance	Bactericidal ions and concentration (μg/L)	Degradation rate	Cultured cell; viability; extraction concentration	Incubation period	Ref.
Zn-0.8Li	*S. epidermidis, S. aureus*	IZD= 13.6 mm	Zn^{2+}, Li^{+}	17 μm/ yr (after 90d)	–	–	[31]
Zn-0.8Li-0.5Ag	*S. epidermidis, S. aureus*	IZD= 24.8 mm	Zn^{2+}, Li^{+}, Ag^{+}	19.5 μm/ yr (after 90d)	–	–	[31]
Zn-0.8Li-1.25Ag	*S. epidermidis, S. aureus*	IZD= 18.4 mm	Zn^{2+}, Li^{+}, Ag^{+}	18 μm/ yr (after 90d)	–	–	[31]
Zn-0.8Li-1.2.0Ag	*S. epidermidis, S. aureus*	IZD= 25.3 mm	Zn^{2+}, Li^{+}, Ag^{+}	16 μm/ yr (after 90d)	–	–	[31]
Zn foam	*S. aureus*	IZD= 5.85 mm	Zn^{2+}= 6200	1.3 ± 0.2 mg/d	MC3T3 & MG63; 75% & 81%; at 25%	3d	[191]
ZnO+Zn foam	*S. aureus*	IZD= 6.15 mm	Zn^{2+}= 4200	1.0 ± 0.1 mg/d	MC3T3 & MG63; 76% & 82.5%; at 25%	3d	[191]
ZnP+Zn foam	*S. aureus*	IZD= 5.40 mm	Zn^{2+}= 3650	0.7 ± 0.2 mg/d	MC3T3 & MG63; 92% & 90%; at 25%	3d	[191]
(ZnO+ZnP)+ Zn foam	*S. aureus*	IZD= 6.0 mm	Zn^{2+}=3150	0.5 ± 0.1 mg/d	MC3T3 & MG63; 95% & 89%; at 25%	3d	[191]
Sr-Ca-P-Zn1 (Zn doped)	*E. coli, S. aureus*	Antibacterial rates. 59% for *S. aureus;* 52% for *E. coli*	Zn^{2+}= 156 ppb after 100 h	14.2 μm/ yr (after 30d)	MC3T3; 91%; co-culture	5d	[192]
Sr-Ca-P-Zn4 (Zn doped)	*E. coli, S. aureus*	Antibacterial rates. 80% for *S. aureus; 71%* for *E. coli*	Zn^{2+}= 205 ppb after 100 h	16.3 μm/ yr (after 30d)	MC3T3; 91%; co-culture	5d	[192]
Zn-Dy (HR)	*S. aureus*	IZD= 5.2 mm	Zn^{2+}= 0.8 μg/mL Dy^{3+}= 5 ng/mL	38 μm/ yr (after 30d)	MC3T3-E1; 68%; at 25%	3d	[174]
Zn-3Dy (HR)	*S. aureus*	IZD= 6.4 mm	Zn^{2+}= 0.83 μg/mL Dy^{3+}= 22 ng/mL	40 μm/ yr (after 30d)	MC3T3-E1; 75%; at 25%	3d	[174]
Zn-5Dy (HR)	*S. aureus*	IZD= 7.3 mm	Zn^{2+}= 0.9 μg/mL Dy^{3+}= 38 ng/mL	49 μm/ yr (after 30 days)	MC3T3-E1; 70%; at 25%	3d	[174]

*PEO-plasma electrolytic oxidation, NIR: near-infrared light, APC- aliphatic polycarbonate, HEV- Hydrogen evolution volume, GO-Graphene oxide, IZD- Inhibition zone diameter.

Please cite this article as: C.A. Shahed, F. Ahmad, E. Günister et al., Antibacterial mechanism with consequent cytotoxicity of different reinforcements in biodegradable magnesium and zinc alloys: A review, Journal of Magnesium and Alloys, https://doi.org/10.1016/j.jma.2023.08.018

7. Conclusion

- Bacterial infections are a severe concern to biomedical materials associated with unsuccessful implants, loss of bone density, and necrosis. Mg and Zn are considered the two most suitable materials for biodegradable implants with antibacterial properties. Pure Mg and Zn generally suffer from rapid degradation and loss of quick mechanical strength for most implant-related applications. Also, Mg^{2+} and Zn^{2+} ions do not show antibacterial efficacy against metal-resistant strain bacteria like *P. Aeruginosa*.
- Although a porous surface helps osseointegration, excessive degradation of implants causes H_2 evolution, hypermagnesemia, and osmotic pressure that can harm human cells. Introducing hydrophobic surface by anodic oxidation, annealing at a higher temperature can resolve excessive degradation.
- Different metal ions have different antibacterial mechanisms, such as Ag ions creating bonds with thiol enzyme, DNA, and RNA to kill bacteria, whereas Ag NPs block the Na and K ion transportation. Soluble Cu^{2+} ions extract electrons from the phospholipid and break the cell membrane; hence, it can inhibit the growth of MRSC bacteria. Ga^{3+} ions resist bacteria from absorbing their essential Fe^{3+} ions.
- Additional antibacterial elements, e.g., CuO, MgO, TiO_2, ZnO, and ZnO NPs, have synergic effects of inhibiting bacterial growth effectively. The bactericidal efficacy is higher for nanoparticles as they directly attack the cytoplasm, DNA, and RNA of the bacteria by penetrating the cell envelope. TiO_2 and ZnO NPs convert H_2O and O_2 to ROS products, which can damage bacterial protein and DNA by oxidation. It also bonds with the receptors and prevents the bacteria from absorbing nutrients.
- Li has selected antibacterial properties like $Ag^{+,}$ but the main attraction is that it activates the WCS pathway to accelerate cell proliferation. Transitional metal ions like Cr, V, Zr, and Sr also show mediocre antibacterial performance. Photothermal properties of black Mn-LDH nanosheet and sodium copper chlorophyllin could be the future of controlled target killing of bacteria.
- It has been observed that metal from Group 1 and Group 2 of the periodic table shows superior antibacterial properties by forming hydroxyl radicles. Besides, a correlation has been observed between the oxidation number and the antibacterial efficacy in the order of $+1 > +2 > +3$.

CRediT author statement

Chowdhury Ahmed Shahed: Conceptualization, Formal analysis, Writing-original draft preparation. Faiz Ahmad: Resources, Supervision. Ebru Günister: Writing- reviewing first and final draft and editing. Farhana Mohd Foudzi: Writing- reviewing the first draft and editing, Saad Ali: Writing- reviewing final draft and editing, Khurshid Malik: Writing- reviewing final draft and editing, Wan Sharuzi Wan Harun: Writing-reviewing final draft and editing,

Declaration of Competing Interest

The authors declare that they have no known competing financial interests or personal relationships that could have appeared to influence the work reported in this paper

Acknowledgement

The authors acknowledge the provided funding support by Universiti Teknologi PETRONAS (UTP), Malaysia, under Grant No. 015LC0-336.

References

[1] V. Tsakiris, C. Tardei, F.M. Clicinschi, J. Magnes. Alloys 9 (6) (2021) 1884–1905, doi:10.1016/j.jma.2021.06.024.
[2] K. Schlichting, M. Dahne, A.J.S.m. Weiler, a. review, Sports Med. Arthrosc. 14 (3) (2006) 169–176, doi:10.1097/00132585-200609000-00009.
[3] M. Prakasam, J. Locs, K. Salma-Ancane, D. Loca, A. Largeteau, L. Berzina-Cimdina, J. Funct. Biomater. 8 (4) (2017) 44, doi:10.3390/jfb8040044.
[4] B. Deng, et al., Materials 14 (14) (2021) 3784, doi:10.3390/ma14143784.
[5] Y. Guo, et al., Adv. Eng. Mater. 23 (4) (2021) 2001000, doi:10.1002/adem.202001000.
[6] M. Schinhammer, I. Gerber, A.C. Hänzi, P.J. Uggowitzer, Mater. Sci. Eng.: C 33 (2) (2013) 782–789 2013/03/01/, doi:10.1016/j.msec.2012.11.002.
[7] J.-H. Chen, C. Liu, L. You, C.A. Simmons, J. Biomech. 43 (1) (2010) 108–118, doi:10.1016/j.jbiomech.2009.09.016.
[8] A. Sas, P. Pellikaan, S. Kolk, P. Marty, T. Scheerlinck, G.H. Van Lenthe, J. Orthop. Res. 37 (3) (2019) 681–688, doi:10.1002/jor.24240.
[9] A. Gungor, A. Incesu, J. Magnes. Alloys 9 (1) (2021) 241–253 2021/01/15/, doi:10.1016/j.jma.2020.09.009.
[10] M. Niinomi, Metals for Biomedical Devices, 2nd ed., Woodhead publishing, 2019.
[11] S. Kamrani, C.J.B. Fleck, Biometals 32 (2) (2019) 185–193, doi:10.1007/s10534-019-00170-y.
[12] Y.F. Zheng, X.N. Gu, F.J.M.S. Witte, E.R. Reports, Mater. Sci. Eng.: R: Reports 77 (2014) 1–34, doi:10.1016/j.mser.2014.01.001.
[13] Q. Chen, G.A.J.M.S. Thouas, E.R. Reports, Mater. Sci. Eng.: R: Reports 87 (2015) 1–57, doi:10.1016/j.mser.2014.10.001.
[14] X. Yan, et al., Corros. Sci. 156 (2019) 125–138 2019/08/01/, doi:10.1016/j.corsci.2019.05.015.
[15] W. Zhang, et al., J. Magnes. Alloys (2022) 2022/02/05/, doi:10.1016/j.jma.2021.12.013.
[16] Y. Yang, X. Xiong, J. Chen, X. Peng, D. Chen, F. Pan, J. Magnes. Alloys 9 (3) (2021) 705–747 2021/05/15/, doi:10.1016/j.jma.2021.04.001.
[17] S. González, E. Pellicer, S. Suriñach, M. Baró, J. Sort, in: Biodegradation-Engineering and Technology, IntechOpen, 2013, pp. 313–340.
[18] Y. Yun, et al., Mater. Today 12 (10) (2009) 22–32, doi:10.1016/S1369-7021(09)70273-1.
[19] P. Tong, et al., Int. J. Biol. Macromol. 237 (2023) 124191 2023/05/15/, doi:10.1016/j.ijbiomac.2023.124191.
[20] A.A. Oliver, et al., ACS Appl. Bio Mater. 3 (10) (2020) 6779–6789, doi:10.1021/acsabm.0c00740.
[21] J. Cao, N.T. Kirkland, K. Laws, N. Birbilis, M.J.A.b. Ferry, Acta Biomater. 8 (6) (2012) 2375–2383, doi:10.1016/j.actbio.2012.03.009.
[22] H. Li, et al., Sci. Rep. 5 (1) (2015) 1–14, doi:10.1038/srep10719.
[23] G. Katarivas Levy, J. Goldman, E.J.M. Aghion, Metals 7 (10) (2017) 402, doi:10.3390/met7100402.
[24] M. Sikora-Jasinska, et al., Mater. Sci. Eng.: C 77 (2017) 1170–1181, doi:10.1016/j.msec.2017.04.023.

[25] Y. Meng, et al., Bioact. Mater. 4 (2019) 87–96 2019/12/01/, doi:10.1016/j.bioactmat.2018.08.003.
[26] L. Tan, X. Yu, P. Wan, K. Yang, Technology, J. Mater. Sci. Technol. 29 (6) (2013) 503–513, doi:10.1016/j.jmst.2013.03.002.
[27] Y. Hou, X. Zhang, J. Li, L. Wang, S. Guan, J. Magnes. Alloys (2022) 2022/07/10/, doi:10.1016/j.jma.2022.06.008.
[28] M.-S. Song, et al., J. Mater. Sci. Technol. 35 (4) (2019) 535–544 2019/04/01/, doi:10.1016/j.jmst.2018.10.008.
[29] X. He, X. Zhang, X. Wang, L. Qin, Coatings 7 (3) (2017) 45, doi:10.3390/coatings7030045.
[30] N. Kavanagh, et al., Clin. Microbiol. Rev. 31 (2) (2018), doi:10.1128/cmr.00084-17.
[31] B. Jia, et al., Biomaterials 287 (2022) 121663 2022/08/01/, doi:10.1016/j.biomaterials.2022.121663.
[32] Z. Lin, X. Sun, H. Yang, Mater. Des. 198 (2021) 109350, doi:10.1016/j.matdes.2020.109350.
[33] E. Abkar, M. Hassanpour, O. Amiri, M. Ghanbari, M. Salavati-Niasari, RSC Adv. 11 (36) (2021) 22238–22249, doi:10.1039/D1RA03666A.
[34] R. Krishnan, et al., J. Mater. Res. Technol. (2022), doi:10.1016/j.jmrt.2022.06.178.
[35] Q. Liu, et al., J. Funct. Biomater. 14 (4) (2023) 206, doi:10.3390/jfb14040206.
[36] C. Junqueira, et al., Nat. Immunol. 22 (3) (2021) 347–357 2021/03/01, doi:10.1038/s41590-020-00847-4.
[37] P.M. Sullivan, C. Takao, N.D. Patel, F.F. Ing, J. Soc. Cardiovasc. Angiography Interv. 2 (2) (2023) 100547 2023/03/01/, doi:10.1016/j.jscai.2022.100547.
[38] E.L. Meier, Y. Jang, Curr. Opin. Biomed. Eng. (2023) 100448, doi:10.1016/j.cobme.2023.100448.
[39] X. Chen, J. Zhou, Y. Qian, L. Zhao, Mater. Today Bio (2023) 100586, doi:10.1016/j.mtbio.2023.100586.
[40] B. Venkateswarlu, B.R. Sunil, R.S. Kumar, Materialia (2023) 101680, doi:10.1016/j.mtla.2023.101680.
[41] J. Jiao, S. Zhang, X. Qu, B. Yue, Front. Cell. Infect. Microbiol. 11 (2021) 693939, doi:10.3389/fcimb.2021.693939.
[42] M. Nasr Azadani, A. Zahedi, O.K. Bowoto, B.I. Oladapo, Prog Biomater. 11 (1) (2022) 1–26 2022/03/01, doi:10.1007/s40204-022-00182-x.
[43] J.C. Paiva, L. Oliveira, M.F. Vaz, S. Costa-de-Oliveira, Bioeng. 9 (8) (2022) 409, doi:10.3390/bioengineering9080409.
[44] J. Spałek, et al., Int. J. Mol. Sci. 23 (5) (2022) 2575, doi:10.3390/ijms23052575.
[45] M. Salama, M.F. Vaz, R. Colaço, C. Santos, M. Carmezim, J. Funct. Biomater. 13 (2) (2022) 72, doi:10.3390/jfb13020072.
[46] E. Zhang, X. Zhao, J. Hu, R. Wang, S. Fu, G. Qin, Bioact. Mater. 6 (8) (2021) 2569–2612, doi:10.1016/j.bioactmat.2021.01.030.
[47] Q. Fu, et al., J. Magnes. Alloys (2023) 2023/06/10/, doi:10.1016/j.jma.2023.05.002.
[48] K. Luo, L. Zhang, G. Wu, W. Liu, W. Ding, J. Magnes. Alloys 7 (2) (2019) 345–354, doi:10.1016/j.jma.2019.03.002.
[49] J. Lyu, et al., Mater. Sci. Eng.: A 773 (2020) 138735, doi:10.1016/j.msea.2019.138735.
[50] Ł.J. Robert Karpiński, Paulina Czubacka, J. Technol. Exploit. Mech. Eng. 3 (1) (2017) 43–51, doi:10.35784/jteme.538.
[51] T.H.C. Harvard, The Nutrition Source, Zinc, School of Public Health, 2023 https://www.hsph.harvard.edu/nutritionsource/zinc/#:~:text=Meats%2C%20poultry%2C%20and%20seafood%20are,the%20mineral%2C%20lowering%20its%20absorption (accessed 28 April).
[52] P. Wang, et al., Colloids Surf. B 173 (2019) 512–520, doi:10.1016/j.colsurfb.2018.10.027.
[53] V.P. Shiju, N.V. Abhijith, U. Sudeep, J. Phys. Conf. Ser. 1355 (1) (2019) 012028 2019/11/01 10.1088/1742-6596/1355/1/012028 .
[54] X.L. Liu, W.R. Zhou, Y.H. Wu, Y. Cheng, Y.F. Zheng, Mater. Sci. Eng.: C 33 (7) (2013) 4144–4154 2013/10/01/, doi:10.1016/j.msec.2013.06.004.
[55] F. Peng, et al., ACS Omega 6 (14) (2021) 9843–9851 2021/04/13, doi:10.1021/acsomega.1c00531.
[56] Y. Liu, W. Yao, X. Yin, H. Wang, Z. Han, L. Ren, Adv. Mater. Interfaces 3 (8) (2016) 1500723, doi:10.1002/admi.201500723.
[57] A. Kudyba, W. Polkowski, G. Bruzda, A. Polkowska, D. Giuranno, J. Magnes. Alloys 10 (11) (2022) 3133–3142 2022/11/01/, doi:10.1016/j.jma.2021.10.003.
[58] V.P. Chavda, G. Jogi, A.C. Paiva-Santos, A. Kaushik, Expert Opin. Drug Deliv. 19 (10) (2022) 1177–1181, doi:10.1080/17425247.2022.2110065.
[59] T. Khodaei, E. Schmitzer, A.P. Suresh, A.P. Acharya, Bioact. Mater. 24 (2023) 153–170 2023/06/01/, doi:10.1016/j.bioactmat.2022.12.012.
[60] L. Jin, et al., Front. Immunol. 10 (2019) 2798, doi:10.3389/fimmu.2019.02798.
[61] M.D. Costantino, A. Schuster, H. Helmholz, A. Meyer-Rachner, R. Willumeit-Römer, B.J.C. Luthringer-Feyerabend, Acta Biomater. 101 (2020) 598–608 2020/01/01/, doi:10.1016/j.actbio.2019.10.014.
[62] R.J. Guillory, A.A. Oliver, E.K. Davis, E.J. Earley, J.W. Drelich, J. Goldman, JOM 71 (2019) 1436–1446, doi:10.1007/s11837-019-03371-5.
[63] H. Jin, et al., Mater. Sci. Eng.: C 84 (2018) 67–79 2018/03/01/, doi:10.1016/j.msec.2017.11.021.
[64] S. Zhao, et al., Mater. Sci. Eng.: C 76 (2017) 301–312 2017/07/01/, doi:10.1016/j.msec.2017.02.167.
[65] R.J. Guillory, et al., ACS Biomater. Sci. Eng. 2 (12) (2016) 2355–2364, doi:10.1021/acsbiomaterials.6b00591.
[66] H. Qiang, et al., Regen. Biomater. 10 (2023) rbad051, doi:10.1093/rb/rbad051.
[67] C. Zhou, et al., Acta Biomater. 97 (2019) 657–670 2019/10/01/, doi:10.1016/j.actbio.2019.08.012.
[68] J. Niu, et al., Mater. Sci. Eng.: C 69 (2016) 407–413, doi:10.1016/j.msec.2016.06.082.
[69] D. Zhao, et al., JOM 68 (2016) 1204–1208, doi:10.1007/s11837-015-1775-z.
[70] A. Kumar, P.M. Pandey, J. Alloys Compd. 854 (2021) 156211, doi:10.1016/j.jallcom.2020.156211.
[71] D.J. Hickey, B. Ercan, S. Chung, T.J. Webster, L. Sun, B. Geilich, in: 2014 40th Annual Northeast Bioengineering Conference (NEBEC), 2014, pp. 1–2, doi:10.1109/NEBEC.2014.6972815. 25-27 April 2014.
[72] Y. Xin, T. Hu, P. Chu, Acta Biomater. 7 (4) (2011) 1452–1459, doi:10.1016/j.actbio.2010.12.004.
[73] K. Chen, et al., Bioact. Mater. 5 (2) (2020) 275–285 2020/06/01/, doi:10.1016/j.bioactmat.2020.02.014.
[74] J. Gonzalez, R.Q. Hou, E.P. Nidadavolu, R. Willumeit-Römer, F. Feyerabend, Bioact. Mater. 3 (2) (2018) 174–185, doi:10.1016/j.bioactmat.2018.01.003.
[75] M. Razavi, et al., Ceram. Int. 40 (3) (2014) 3865–3872, doi:10.1016/j.ceramint.2013.08.027.
[76] H. Kabir, K. Munir, C. Wen, Y. Li, Bioact. Mater. 6 (3) (2021) 836–879 2021/03/01/, doi:10.1016/j.bioactmat.2020.09.013.
[77] P.K. Bowen, A. Drelich, J. Drelich, J. Goldman, J. Biomed. Mater. Res. Part A 103 (1) (2015) 341–349, doi:10.1002/jbm.a.35179.
[78] H.F. Li, et al., Sci. Rep. 5 (1) (2015) 10719 2015/05/29, doi:10.1038/srep10719.
[79] D. Mei, et al., J. Magnes. Alloys (2023) 2023/05/20/, doi:10.1016/j.jma.2023.04.006.
[80] P. Li, et al., Acta Biomater. 98 (2019) 235–245 2019/10/15/, doi:10.1016/j.actbio.2019.03.013.
[81] H. Matusiewicz, Acta Biomater. 10 (6) (2014) 2379–2403 2014/06/01/, doi:10.1016/j.actbio.2014.02.027.
[82] D. Xue, Y. Yun, Z. Tan, Z. Dong, M.J. Schulz, J. Mater. Sci. Technol. 28 (3) (2012) 261–267 2012/03/01/, doi:10.1016/S1005-0302(12)60051-6.
[83] X. Chen, J. Zhou, Y. Qian, L. Zhao, Mater. Today Bio 19 (2023) 100586 2023/04/01/, doi:10.1016/j.mtbio.2023.100586.
[84] L.-Y. Li, et al., Acta Biomater. 79 (2018) 23–36, doi:10.1016/j.actbio.2018.08.030.
[85] Y. Shao, et al., Acta Metall. Sin. 33 (2020) 615–629 *(English Letters)*, doi:10.1007/s40195-020-01044-w.

Please cite this article as: C.A. Shahed, F. Ahmad, E. Günister et al., Antibacterial mechanism with consequent cytotoxicity of different reinforcements in biodegradable magnesium and zinc alloys: A review, Journal of Magnesium and Alloys, https://doi.org/10.1016/j.jma.2023.08.018

[86] J. Rodríguez-Sánchez, M.Á. Pacha-Olivenza, M.L. González-Martín, Mater. Chem. Phys. 221 (2019) 342–348, doi:10.1016/j.matchemphys.2018.09.050.
[87] L. Scheideler, et al., Acta Biomater. 9 (10) (2013) 8740–8745 Article, doi:10.1016/j.actbio.2013.02.020.
[88] W. Zhou, et al., Biomater. Sci. 9 (3) (2021) 807–825 10.1039/D0BM01584A, doi:10.1039/D0BM01584A.
[89] S. Hussain, et al., Front. Microbiol. 13 (2022) Review2022-May-31, doi:10.3389/fmicb.2022.900740.
[90] L.M. Plum, L. Rink, H. Haase, J. Environ. Res. Public Health 7 (4) (2010) 1342–1365, doi:10.3390/ijerph7041342.
[91] C. Liao, Y. Jin, Y. Li, S.C. Tjong, Int. J. Mol. Sci. 21 (17) (2020) 6305, doi:10.3390/ijms21176305.
[92] J. Kubásek, D. Vojtěch, E. Jablonská, I. Pospíšilová, J. Lipov, T. Ruml, Mater. Sci. Eng.: C 58 (2016) 24–35, doi:10.1016/j.msec.2015.08.015.
[93] J. Ma, N. Zhao, D. Zhu, ACS Biomater. Sci. Eng. 1 (11) (2015) 1174–1182, doi:10.1021/acsbiomaterials.5b00319.
[94] B. Xie, et al., Int. J. Bioprinting 7 (1) (2020) 300-300, doi:10.18063/ijb.v7i1.300.
[95] D. Li, et al., Acta Biomater. 141 (2022) 454–465, doi:10.1016/j.actbio.2021.12.032.
[96] Y. Zhao, K. Tan, Y. Zhou, Z. Ye, W.-S. Tan, Mater. Sci. Eng.: C 59 (2016) 193–202 2016/02/01/, doi:10.1016/j.msec.2015.10.017.
[97] Y. Li, C. Liu, Nanoscale 9 (15) (2017) 4862–4874 10.1039/C7NR00835J, doi:10.1039/C7NR00835J.
[98] Z. Tan, et al., Stem Cells Int. 2021 (2021) 1–15, doi:10.1155/2021/6662164.
[99] F. He, et al., J. Mater. Chem. B 10 (21) (2022) 4040–4047, doi:10.1039/D2TB00471B.
[100] T.-b. Huang, et al., Biomater. Sci. 7 (3) (2019) 1101–1116, doi:10.1039/C8BM01411F.
[101] M. Arioka, et al., Biochem. Pharmacol. 90 (4) (2014) 397–405, doi:10.1016/j.bcp.2014.06.011.
[102] Y. Liu, B. Rath, M. Tingart, J. Eschweiler, J. Biomed. Mater. Res. Part A 108 (3) (2020) 470–484, doi:10.1002/jbm.a.36829.
[103] Y. Zhao, et al., Biomaterials 34 (37) (2013) 9264–9277, doi:10.1016/j.biomaterials.2013.08.071.
[104] R. Imran, A. Al Rashid, M. Koç, Bioprinting 28 (2022) e00236 2022/12/01/, doi:10.1016/j.bprint.2022.e00236.
[105] Q.L. Feng, J. Wu, G.Q. Chen, F. Cui, T. Kim, J. Kim, J. Biomed. Mater. Res. 52 (4) (2000) 662–668, doi:10.1002/1097-4636(20001215)52:4⟨662::AID-JBM10⟩3.0.CO;2-3.
[106] A. Mocanu, et al., Appl. Surf. Sci. 298 (2014) 225–235, doi:10.1016/j.apsusc.2014.01.166.
[107] D. Tie, et al., Eur. Cell Mater. 25 (2013) 284–298 discussion 298, doi:10.22203/ecm.v025a20.
[108] S. Zhang, C. Du, Z. Wang, X. Han, K. Zhang, L. Liu, Toxicol. in Vitro 27 (2) (2013) 739–744, doi:10.1016/j.tiv.2012.12.003.
[109] X. Qu, et al., Bioact. Mater. 6 (12) (2021) 4607–4624 2021/12/01/, doi:10.1016/j.bioactmat.2021.05.023.
[110] K.B. Törne, F.A. Khan, A. Örnberg, J. Weissenrieder, Surf. Innov. 6 (1–2) (2017) 81–92.
[111] M. Razzaghi, M. Kasiri-Asgarani, H.R. Bakhsheshi-Rad, H. Ghayour, J. Mater. Eng. Perform. 28 (3) (2019) 1441–1455 2019/03/01, doi:10.1007/s11665-019-03923-5.
[112] Z. Liu, et al., Oxid. Med. Cell Longev. 2017 (2017), doi:10.1155/2017/8091265.
[113] Y. Dai, et al., Metals 8 (11) (2018) 948, doi:10.3390/met8110948.
[114] P. Siritongsuk, et al., PLoS One 11 (12) (2016) e0168098, doi:10.1371/journal.pone.0168098.
[115] J.P. Ruparelia, A.K. Chatterjee, S.P. Duttagupta, S. Mukherji, Acta Biomater. 4 (3) (2008) 707–716, doi:10.1016/j.actbio.2007.11.006.
[116] K.-Y. Yoon, J.H. Byeon, J.-H. Park, J. Hwang, Sci. Total Environ. 373 (2–3) (2007) 572–575, doi:10.1016/j.scitotenv.2006.11.007.
[117] D.A. Florea, et al., Int. J. Mol. Sci. 23 (14) (2022) 7910, doi:10.3390/ijms23147910.
[118] J. Rajkumari, S. Busi, A.C. Vasu, P. Reddy, Microb. Pathog. 107 (2017) 261–269 2017/06/01/, doi:10.1016/j.micpath.2017.03.044.
[119] M.K.Y. Soliman, S.S. Salem, M. Abu-Elghait, M.S. Azab, Appl. Biochem. Biotechnol. 195 (2) (2023) 1158–1183 2023/02/01, doi:10.1007/s12010-022-04199-7.
[120] A.R. Gliga, S. Skoglund, I. Odnevall Wallinder, B. Fadeel, H.L. Karlsson, Part. Fibre Toxicol. 11 (1) (2014) 11 2014/02/17, doi:10.1186/1743-8977-11-11.
[121] L. Turell, R. Radi, B. Alvarez, Free Radical Biol. Med. 65 (2013) 244–253 2013/12/01/, doi:10.1016/j.freeradbiomed.2013.05.050.
[122] F.A. Serrano, et al., BMC Cancer 11 (1) (2011) 296 2011/07/14, doi:10.1186/1471-2407-11-296.
[123] I.A. Cotgreave, P. Moldeus, S. Orrenius, Annu. Rev. Pharmacol. Toxicol. 28 (1) (1988) 189–212, doi:10.1146/annurev.pa.28.040188.001201.
[124] H. Ji, et al., J. Alloys Compd. 864 (2021) 158415 2021/05/25/, doi:10.1016/j.jallcom.2020.158415.
[125] C.A.P. Bastos, et al., NanoImpact 17 (2020) 100192 2020/01/01/, doi:10.1016/j.impact.2019.100192.
[126] L. Nan, et al., J. Mater. Sci. Mater. Med. 19 (2008), doi:10.1007/s10856-008-3444-z.
[127] C. Shuai, et al., J. Mater. Sci. Technol. 34 (10) (2018) 1944–1952, doi:10.1016/j.jmst.2018.02.006.
[128] A.K. Chatterjee, R. Chakraborty, T. Basu, Nanotechnology 25 (13) (2014) 135101, doi:10.1088/0957-4484/25/13/135101.
[129] Y. Li, et al., Biomaterials 106 (2016) 250–263, doi:10.1016/j.biomaterials.2016.08.031.
[130] X. Qu, H. Yang, B. Jia, Z. Yu, Y. Zheng, K. Dai, Acta Biomater. 117 (2020) 400–417, doi:10.1016/j.actbio.2020.09.041.
[131] X. Tong, et al., Smart Mater. Manuf. 1 (2023) 100012 2023/01/01/, doi:10.1016/j.smmf.2022.100012.
[132] G.M. Teitzel, M.R. Parsek, Appl. Environ. Microbiol. 69 (4) (2003) 2313–2320, doi:10.1128/AEM.69.4.2313-2320.2003.
[133] X. Tong, et al., Acta Biomater. 102 (2020) 481–492 2020/01/15/, doi:10.1016/j.actbio.2019.11.031.
[134] G. Bao, et al., Acta Biomater. 142 (2022) 374–387 2022/04/01/, doi:10.1016/j.actbio.2022.01.053.
[135] J. Chen, Y. Zhang, M. Ibrahim, I.P. Etim, L. Tan, K. Yang, Colloids Surf. B 179 (2019) 77–86, doi:10.1016/j.colsurfb.2019.03.023.
[136] S. Duan, X. Zhao, Z. Su, C. Wang, Y. Lin, ACS Appl.Bio Mater. 3 (6) (2020) 3673–3680, doi:10.1021/acsabm.0c00300.
[137] A. Awadallah-F, F. Hillman, S.A. Al-Muhtaseb, H.-K. Jeong, J. Mater. Sci. 54 (2019) 5513–5527, doi:10.1007/s10853-018-03249-y.
[138] S. Meghana, P. Kabra, S. Chakraborty, N. Padmavathy, RSC Adv. 5 (16) (2015) 12293–12299, doi:10.1039/C4RA12163E.
[139] L. Ling, et al., Colloids Surf. B 219 (2022) 112810, doi:10.1016/j.colsurfb.2022.112810.
[140] S. Lin, et al., J. Mater. Sci. Mater. Med. 30 (2019) 1–12, doi:10.1007/s10856-019-6324-9.
[141] C. García-Mintegui, et al., Bioact. Mater. 6 (12) (2021) 4430–4446, doi:10.1016/j.bioactmat.2021.04.015.
[142] B.D. Hoyle, J. Alcantara, J.W. Costerton, Antimicrob. Agents Chemother. 36 (9) (1992) 2054–2056, doi:10.1128/aac.36.9.2054.
[143] M. Wątroba, et al., J. Biomed. Mater. Res. Part B: Appl. Biomater. 111 (2) (2023) 241–260 2023/02/01, doi:10.1002/jbm.b.35147.
[144] N. Murni, M. Dambatta, S. Yeap, G. Froemming, H. Hermawan, Mater. Sci. Eng.: C 49 (2015) 560–566, doi:10.1016/j.msec.2015.01.056.
[145] J. Pinc, et al., Mater. Sci. Eng.: A 824 (2021) 141809, doi:10.1016/j.msea.2021.141809.
[146] Y.-K. Shin, Y. Shin, J.W. Lee, M.-H. Seo, Biosensors 12 (11) (2022) 952, doi:10.3390/bios12110952.
[147] C. Zhang, et al., ACS Biomater. Sci. Eng. 6 (1) (2019) 517–538, doi:10.1021/acsbiomaterials.9b00903.
[148] Y.-H. Zou, et al., Acta Biomater. 98 (2019) 196–214, doi:10.1016/j.actbio.2019.05.069.
[149] K. Bhatt, V.K. Jain, F. Khan, J. Indian Chem. Soc. 99 (5) (2022) 100441, doi:10.1016/j.jics.2022.100441.
[150] M.J. Hajipour, et al., Trends Biotechnol. 30 (10) (2012) 499–511 2012/10/01/, doi:10.1016/j.tibtech.2012.06.004.
[151] I.S. Okeke, K.K. Agwu, A.A. Ubachukwu, F.I. Ezema, Appl. Surf. Sci. Adv. 8 (2022) 100227 2022/04/01/, doi:10.1016/j.apsadv.2022.100227.

Please cite this article as: C.A. Shahed, F. Ahmad, E. Günister et al., Antibacterial mechanism with consequent cytotoxicity of different reinforcements in biodegradable magnesium and zinc alloys: A review, Journal of Magnesium and Alloys, https://doi.org/10.1016/j.jma.2023.08.018

[152] R. Kumar, A. Umar, G. Kumar, H.S. Nalwa, Ceram. Int. 43 (5) (2017) 3940–3961, doi:10.1016/j.ceramint.2016.12.062.
[153] S. Jiang, K. Lin, M. Cai, Front. Chem. 8 (2020) Mini Review2020-July-21, doi:10.3389/fchem.2020.00580.
[154] F. Minandri, C. Bonchi, E. Frangipani, F. Imperi, P. Visca, Future Microbiol. 9 (3) (2014) 379–397, doi:10.2217/fmb.14.3.
[155] F. Li, F. Liu, K. Huang, S. Yang, Front. Bioeng. Biotechnol. 10 (2022) Review2022-February-04, doi:10.3389/fbioe.2022.827960.
[156] Y. Zhang, X. Pan, L. Wang, L. Chen, J. Drug Target 29 (3) (2021) 249–258, doi:10.1080/1061186X.2020.1824235.
[157] Z. Lin, C. Gao, D. Wang, Q. He, Angew. Chem. Int. Ed. 60 (16) (2021) 8750–8754, doi:10.1002/anie.202016260.
[158] Z. Gao, et al., Mater. Sci. Eng.: C 104 (2019) 109926, doi:10.1016/j.msec.2019.109926.
[159] M. Vukomanovic, et al., Biomater. Adv. 140 (2022) 213051, doi:10.1016/j.bioadv.2022.213051.
[160] M.A. Akhtar, Z. Hadzhieva, K. Ilyas, M.S. Ali, W. Peukert, A.R. Boccaccini, Pharmaceutics 13 (10) (2021), doi:10.3390/pharmaceutics13101702.
[161] M.A. Akhtar, Z. Hadzhieva, I. Dlouhý, A.R. Boccaccini, Coatings 10 (5) (2020) 483, doi:10.3390/coatings10050483.
[162] M.-S. Song, et al., ACS Biomater. Sci. Eng. 8 (6) (2022) 2709–2723, doi:10.1021/acsbiomaterials.2c00099.
[163] F. Kurtuldu, N. Mutlu, A.R. Boccaccini, D. Galusek, Bioact. Mater. 17 (2022) 125–146, doi:10.1016/j.bioactmat.2021.12.034.
[164] M. Kurtjak, M. Vukomanović, D. Suvorov, Mater. Lett. 193 (2017) 126–129, doi:10.1016/j.matlet.2017.01.092.
[165] T. Keenan, L. Placek, M. Hall, A. Wren, J. Biomed. Mater. Res. Part B: Appl. Biomater. 105 (5) (2017) 1102–1113, doi:10.1002/jbm.b.33655.
[166] S. Pourshahrestani, et al., J. Mater. Chem. B 4 (1) (2016) 71–86, doi:10.1039/C5TB02062J.
[167] T.G. DeLoughery, Med. Clin. 101 (2) (2017) 319–332, doi:10.1016/j.mcna.2016.09.004.
[168] C. Liang, et al., Front. Bioeng. Biotechnol. 9 (2021) 676874, doi:10.3389/fbioe.2021.676874.
[169] Q. Tian, et al., Powder Technol. 371 (2020) 130–141, doi:10.1016/j.powtec.2020.05.031.
[170] A. Puppo, B. Halliwell, Biochem. J. 249 (1) (1988) 185–190, doi:10.1042/bj2490185.
[171] V.D. Chadha, P. Bhalla, D.K.J.L.I. Dhawan, Liver Int. 28 (4) (2008) 558–565, doi:10.1111/j.1478-3231.2008.01674.x.
[172] Y. Qin, et al., Acta Biomater. 142 (2022) 388–401, doi:10.1016/j.actbio.2022.01.049.
[173] Y. Su, et al., Bioact. Mater. 20 (2023) 243–258, doi:10.1016/j.bioactmat.2022.05.033.
[174] X. Tong, et al., Acta Biomater. 155 (2023) 684–702, doi:10.1016/j.actbio.2022.10.053.
[175] S. Ahmadvand, et al., J. Phys. Chem. B 123 (4) (2019) 787–791, doi:10.1021/acs.jpcb.8b10710.
[176] Y. Guo, et al., J. Electrochem. Soc. 165 (14) (2018) C962, doi:10.1149/2.1171814jes.
[177] D. Zhang, et al., Bioact. Mater. 17 (2022) 394–405, doi:10.1016/j.bioactmat.2022.01.032.
[178] Z.-Y. Zhang, et al., Bioact. Mater. 18 (2022) 284–299, doi:10.1016/j.bioactmat.2022.01.050.
[179] L.-Y. Cui, et al., J. Magnes. Alloys 9 (1) (2021) 266–280, doi:10.1016/j.jma.2020.03.009.
[180] W. Gao, B. Feng, Y. Ni, Y. Yang, X. Lu, J. Weng, Appl. Surf. Sci. 257 (2) (2010) 538–546, doi:10.1016/j.apsusc.2010.07.029.
[181] B. Yuan, et al., Bioact. Mater. 18 (2022) 354–367, doi:10.1016/j.bioactmat.2022.02.030.
[182] K. Xie, et al., Bioact. Mater. 8 (2022) 140–152, doi:10.1016/j.bioactmat.2021.06.032.
[183] B. Yuan, et al., Bioact. Mater. 18 (2022) 354–367 2022/12/01/, doi:10.1016/j.bioactmat.2022.02.030.
[184] N. Safari, et al., ACS Biomater. Sci. Eng. 6 (11) (2020) 6253–6262 2020/11/09, doi:10.1021/acsbiomaterials.0c00613.
[185] K. Pan, et al., Chem. Eng. J. 427 (2022) 131596, doi:10.1016/j.cej.2021.131596.
[186] S. Ali, et al., Bioeng. 10 (3) (2023) 302, doi:10.3390/bioengineering10030302.
[187] J. Lin, et al., J. Mater. Sci. Technol. 68 (2021) 76–90 2021/03/30/, doi:10.1016/j.jmst.2020.06.052.
[188] J. Lin, et al., Acta Biomater. 106 (2020) 410–427 2020/04/01/, doi:10.1016/j.actbio.2020.02.017.
[189] Z.-Z. Shi, et al., Mater. Sci. Eng.: C 99 (2019) 969–978 2019/06/01/, doi:10.1016/j.msec.2019.02.044.
[190] X. Tong, et al., Acta Biomater. 146 (2022) 478–494, doi:10.1016/j.actbio.2022.05.017.
[191] L. Zhu, et al., Chem. Eng. J. 450 (2022) 137946 2022/12/15/, doi:10.1016/j.cej.2022.137946.
[192] K. Zuo, et al., ACS Appl. Mater. Interfaces 14 (6) (2022) 7690–7705 2022/02/16, doi:10.1021/acsami.1c23631.
[193] M.M. Markowitz, J. Chem. Educ. 40 (12) (1963) 633, doi:10.1021/ed040p633.
[194] Q. Lei, B. Wang, P. Wang, S. Liu, J. Energy Chem. 38 (2019) 162–169, doi:10.1016/j.jechem.2018.12.022.
[195] A. Hoštacká, I. Čižnár, M. Štefkovičová, Folia Microbiol. 55 (2010) 75–78, doi:10.1007/s12223-010-0012-y.
[196] C. Ratzke, J. Gore, PLoS Biol. 16 (3) (2018) e2004248, doi:10.1371/journal.pbio.2004248.
[197] T.E. Cheatham, P.A. Kollman, J. Am. Chem. Soc. 119 (21) (1997) 4805–4825, doi:10.1021/ja963641w.
[198] D.S. Marynick, H. Schaefer 3rd, Proc. Natl. Acad. Sci. USA. 72 (10) (1975) 3794–3798, doi:10.1073/pnas.72.10.3794.
[199] S. Durdu, et al., J. Mater. Sci. 57 (36) (2022) 17203–17218 2022/09/01, doi:10.1007/s10853-022-07743-2.
[200] R. Sun, L. Casali, R.J. Turner, D. Braga, and F. Grepioni, *Molecules*, 2023, vol. 28, no. 3, https://doi.org/10.3390/molecules28031244.